PLOS Computational Biology

RESEARCH ARTICLE

How cells tame noise while maintaining ultrasensitive transcriptional responses

Eui Min Jeong[1,2☯*], **Chang Yoon Chung**[2,3☯], **Jae Kyoung Kim**[2,4,5,6¤*]

1 Department of Data Science, Inha University, Incheon, Republic of Korea, **2** Biomedical Mathematics Group, Pioneer Research Center for Mathematical and Computational Sciences, Institute for Basic Science, Daejeon, Republic of Korea, **3** Department of Mathematics and Statistics, Université de Montréal, Montréal, Québec, Canada, **4** Department of Mathematical Sciences, KAIST, Daejeon, Republic of Korea, **5** Department of Medicine, College of Medicine, Korea University, Seoul, Republic of Korea, **6** Graduate School of Data Science, KAIST, Daejeon, Republic of Korea

☯ These authors contributed equally to this work.
¤ Current Address: Department of Mathematical Sciences, KAIST, 291, Daehak-ro Yuseong-gu, Daejeon Republic of Korea
* wjddmlals11@inha.ac.kr, jaekkim@kaist.ac.kr

Citation: Jeong EM, Chung CY, Kim JK (2025) How cells tame noise while maintaining ultrasensitive transcriptional responses. PLoS Comput Biol 21(12): e1013217. https://doi.org/10.1371/journal.pcbi.1013217

Editor: Christopher E Miles, University of Utah, UNITED STATES OF AMERICA

Received: June 24, 2025

Accepted: December 3, 2025

Published: December 11, 2025

Peer Review History: PLOS recognizes the benefits of transparency in the peer review process; therefore, we enable the publication of all of the content of peer review and author responses alongside final, published articles. The editorial history of this article is available here: https://doi.org/10.1371/journal.pcbi.1013217

Abstract

Ultrasensitive transcriptional switches are essential for converting gradual molecular inputs into decisive gene expression responses, enabling critical behaviors such as bistability and oscillations. While cooperative binding, relying on direct repressor-DNA binding, has been classically regarded as a key ultrasensitivity mechanism, recent theoretical works have demonstrated that combinations of indirect repression mechanisms—sequestration, blocking, and displacement—can also achieve ultrasensitive switches with greater robustness to transcriptional noise. However, these previous works have neglected key biological constraints such as DNA binding kinetics and the limited availability of transcriptional activators, raising the question of whether ultrasensitivity and noise robustness can be sustained under biologically realistic conditions. Here, we systematically assess the impact of these factors on ultrasensitivity and noise robustness under physiologically plausible conditions. We show that while various repression combinations can reduce noise, only the full combination of all three indirect mechanisms consistently maintains low noise and high ultrasensitivity. As a result, biological oscillators employing this triple repression architecture retain precise rhythmic switching even under high noise, and even when activators are shared across thousands of target genes. Our findings offer a mechanistic explanation for the frequent co-occurrence of these repression mechanisms in natural gene regulatory systems.

Data availability statement: All relevant code for data generation and analysis in this study is available at https://github.com/Mathbiomed/Ultrasensitive-gene-switch.

Funding: The research was supported by the following agencies and institutions: the Institute for Basic Science (grant no. IBS-R029-C3, J.K.K.); Samsung Science and Technology Foundation (grant no. SSTF-BA1902-01, J.K.K.); the National Research Foundation of Korea (NRF) grant funded by the Korean government (MSIT) (grant no. RS-2022-NR068758, J.K.K.); Basic Science Research Program through the National Research Foundation of Korea (NRF) funded by the Ministry of Education (grant no. RS-2025-25397599, J.K.K.); INHA UNIVEERSITY Research Grant (E.M.J.). The funders had no role in study design, data collection and analysis, decision to publish, or preparation of the manuscript.

Competing interests: The authors have declared that no competing interests exist.

Author summary

Cells must make accurate decisions in noisy environments using limited molecular resources. One essential tool for this is the ultrasensitive transcriptional switch, which enables sharp transitions in gene expression. While cooperative binding has long been viewed as the primary mechanism behind ultrasensitivity, it is highly sensitive to molecular noise. Our study explores how cells overcome this limitation by combining three indirect repression mechanisms: sequestration, blocking, and displacement. We show that this triple-repression architecture not only generates ultrasensitivity but also ensures noise robustness under physiologically realistic conditions—even when a single pool of transcription factors regulates thousands of genes. These findings reveal a biologically feasible strategy for noise-resilient transcription and offer a mechanistic explanation for why these repression strategies frequently co-occur in natural systems.

Introduction

Ultrasensitivity, characterized by a sharp output change in response to a small variation in input, underlies many essential regulatory functions in biological systems, including signal amplification, bistability, and oscillatory dynamics [1–4]. One of the most well-known mechanisms that produce ultrasensitive responses is cooperative binding, which is broadly observed across biology, in phenomena such as receptor-ligand binding [5,6], protein–RNA interactions [7], and small-molecule binding [8]. A prominent example in transcriptional regulation is the cooperative binding of repressors to multiple DNA sites, which enables the formation of sharp transcriptional switches, where small changes in repressor concentration lead to abrupt transcriptional repression [9,10]. While a cooperative binding mechanism has traditionally been considered a primary strategy for achieving ultrasensitivity, recent theoretical studies have highlighted alternative approaches [11–20]. In particular, combinations of indirect repression mechanisms—such as sequestration, blocking, and displacement—have been shown through ordinary differential equation (ODE) models to produce comparably strong ultrasensitive responses without requiring direct DNA binding [21]. Building on this, stochastic modeling studies further revealed that unlike cooperative binding, which is susceptible to transcriptional noise, systems employing multiple indirect repression mechanisms exhibit enhanced noise robustness [22]. Collectively, these findings suggest that combinations of indirect repression mechanisms can generate ultrasensitive transcriptional switches that are more robust to noise than a cooperative binding mechanism.

However, these previous studies typically assumed fixed or idealized conditions, without explicitly accounting for key biological parameters such as DNA binding/unbinding rates and the abundance of transcriptional activators [21,22]. In living cells, the kinetics of molecular interactions and the limited availability of regulatory proteins impose significant constraints on transcriptional dynamics [23–25]. It remains unclear

whether ultrasensitivity and noise robustness can still be achieved under such physiologically realistic conditions. Moreover, it is unknown which combinations of repression mechanisms, if any, are capable of maintaining performance under these constraints. Addressing this gap is crucial for understanding how biological systems maintain both precision and sensitivity in gene regulation despite molecular noise and finite resources.

To address this, we explicitly incorporated DNA binding rates and activator copy numbers into the models and systematically evaluated how these biologically constrained parameters impact ultrasensitivity and noise robustness. Our results show that, regardless of the specific repression mechanism, indirect repression can reduce noise when DNA binding is fast and activators are abundant, indicating that previous conclusions [22] were incomplete. However, only the full combination of all three mechanisms consistently achieves low noise levels and high ultrasensitivity within physiologically plausible constraints. Accordingly, biological oscillators employing this triple repression architecture can generate precise rhythms, reliably toggling the transcriptional switch on and off even in the presence of stochastic fluctuations. We further demonstrate that this robustness is preserved even when a single pool of activators simultaneously regulates thousands of target genes rather than a single gene, highlighting the scalability and efficiency of this architecture under conditions mimicking a natural gene regulatory network. These findings offer a mechanistic rationale for the frequent co-occurrence of sequestration, blocking, and displacement in natural transcriptional circuits and present a design principle for constructing resource-efficient and noise-resilient gene regulatory systems.

Results

Ultrasensitivity generated with cooperative binding is noisy

The cooperative binding mechanism, in which the transcriptional repressors bind cooperatively to multiple DNA sites to inhibit transcription, is one of the most common transcriptional mechanisms for generating ultrasensitivity [5,9–11,26]. To achieve an ultrasensitive transcriptional response, we used a model describing the cooperative binding with four independent binding sites (Fig 1a). In the model, free DNA (E_{0000}) contains four binding sites, where repressors (R) bind at a rate of k_f and unbind with rates of k_r, ck_r, c^2k_r, and c^3k_r, for cases in which one (E_{0001}, E_{0010}, E_{0100}, and E_{1000}), two (E_{1100}, E_{1010}, E_{1001}, E_{0110}, E_{0101}, and E_{0011}), three (E_{1110}, E_{1101}, E_{1011}, and E_{0111}), and all four (E_{1111}) sites are occupied by R, respectively. When all sites are occupied, transcription is inhibited, but it remains active when at least one site is unoccupied, producing mRNA at a rate of α, which degrades at a rate of β (Table 1). Thus, the transcriptional activity (i.e., the probability at which the transcription is active), derived using the chemical master equation (CME) framework (see Methods), decreases as the number of repressors (R_T) increases. Notably, the transcriptional activity can be changed sensitively with respect to changes in R_T in the presence of cooperativity (i.e., $c < 1$), achieving ultrasensitivity comparable to the Hill exponent of four (Fig 1b).

This ultrasensitivity is maintained as long as the dissociation constant $K_r = k_r/k_f$ remains fixed, even when k_f varies. However, the noise level changes when k_f varies. For instance, as $k_f = 6 \times 10^2$ is increased to $k_f = 6 \times 10^5$, while keeping $K_r = 10^{-2}$, the level of ultrasensitivity does not change (Fig 1b), but the noise level quantified with the Fano factor (i.e., variance/mean) of the mRNA copy numbers considerably decreases (Fig 1c). To investigate how increasing the values of k_f and k_r attenuates transcriptional noise, we simulated the stationary distribution of mRNA copy numbers (Fig 1d) using the Gillespie algorithm (see Methods) [27]. When k_f and k_r became slow relative to the rates of mRNA production and degradation (i.e., α and β), slow transitions between the active and repressed DNA states resulted in bimodal mRNA stationary distributions (Fig 1d, top). Such noise attenuation by fast k_f and k_r was also observed in an activator model, where transcription occurs only when an activator protein binds cooperatively to all four sites (S1 Fig), consistent with Sánchez *et al* [28].

Next, we investigate whether the noise level in transcription decreases as the binding and unbinding rates become faster across a broad parameter range. For this, while keeping $K_r = 10^{-2}$ and $\alpha/\beta = 100$, we varied k_f and β. We found

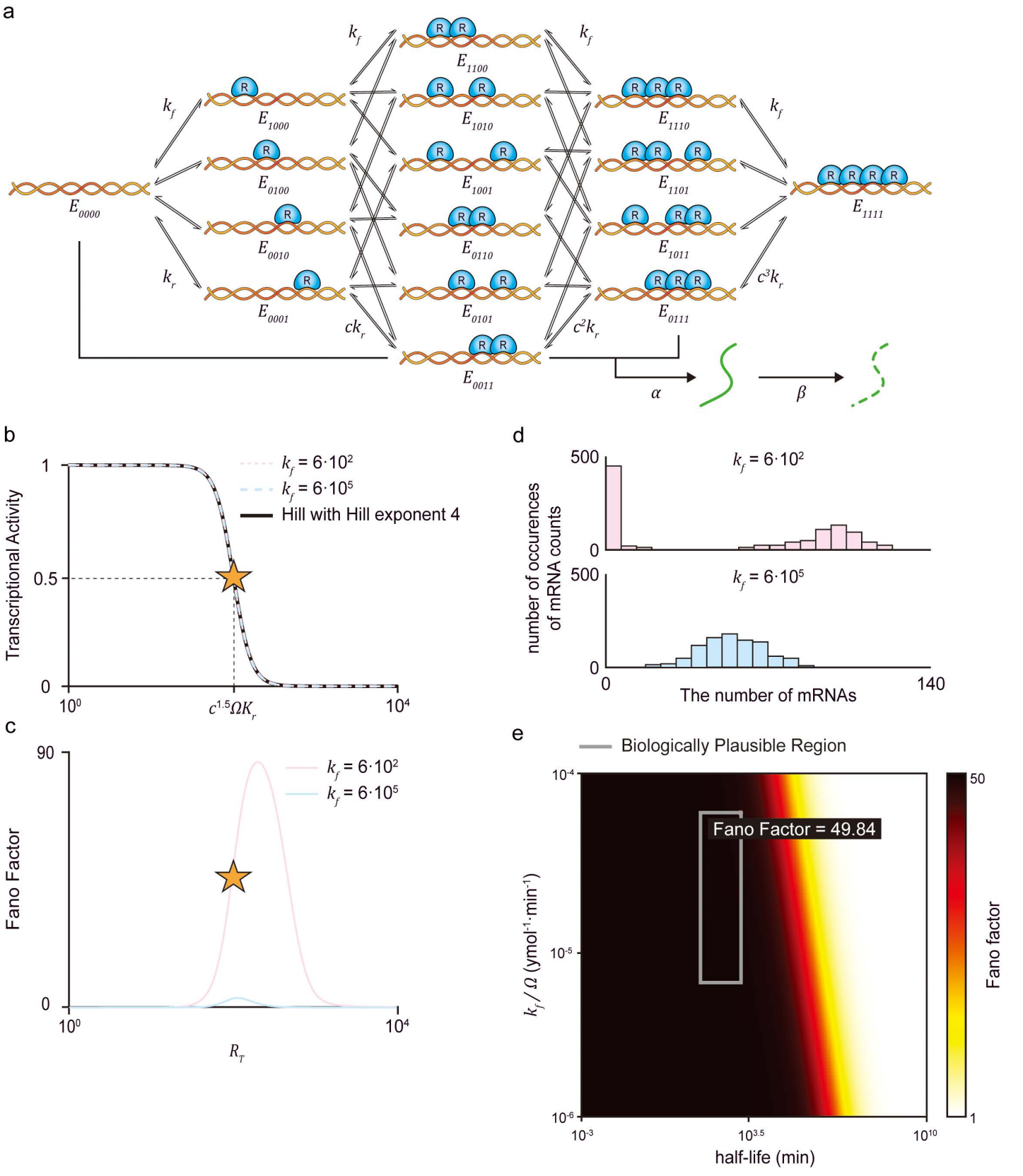
a
k_f
k_r
ck_r
c^2k_r
c^3k_r
E_{0000}
E_{1000}
E_{0100}
E_{0010}
E_{0001}
E_{1100}
E_{1010}
E_{1001}
E_{0110}
E_{0101}
E_{0011}
E_{1110}
E_{1101}
E_{1011}
E_{0111}
E_{1111}
R
α
β
b
Transcriptional Activity
1
0.5
0
10^0
$c^{1.5}\Omega K_r$
10^4
$k_f = 6{\cdot}10^2$
$k_f = 6{\cdot}10^5$
Hill with Hill exponent 4
c
Fano Factor
90
0
10^0
10^4
R_T
$k_f = 6{\cdot}10^2$
$k_f = 6{\cdot}10^5$
d
number of occurences of mRNA counts
500
0
$k_f = 6{\cdot}10^2$
500
0
$k_f = 6{\cdot}10^5$
0
140
The number of mRNAs
e
Biologically Plausible Region
Fano Factor = 49.84
10^{-4}
10^{-5}
10^{-6}
k_f / Ω (ymol^{-1}·min^{-1})
10^{-3}
$10^{3.5}$
10^{10}
half-life (min)
50
1
Fano factor

Fig 1. The cooperative binding mechanism is sensitive to noise under biologically realistic conditions. (a) Model diagram of the transcription regulated by the repressor proteins (R) binding to four independent sites on the DNA within a cell volume of Ω. Each binding site is occupied by R at a rate k_f. Conversely, R unbinds from DNA at a rate k_r when one site is occupied, with the dissociation constant between R and DNA defined as $K_r = k_r/k_f$. For two, three, or four occupied sites, R unbinds at rates of ck_r, c^2k_r, and c^3k_r, respectively. Accordingly, when $c < 1$, cooperative binding is present. When all binding sites are occupied, transcription is inhibited. On the other hand, when any sites remain unoccupied, mRNA is produced at a rate α and degrades at a rate β. (b) When $c = 10^{-2}$, transcriptional activity closely resembles the Hill function with Hill exponent of 4 (black line). Furthermore, transcriptional activity remains consistent with the Hill function regardless of k_f values, provided K_r is kept constant (blue dashed line and red dashed line). (c) Nevertheless, the overall noise level quantified by the Fano factor of mRNAs shows significant differences based on k_f. Such differences are particularly evident when transcriptional activity undergoes sensitive response. Notably, the overall noise levels are reduced during the sensitive response when k_f is faster (blue solid line) compared to when it is slower (red solid line). (d) To investigate how differences in k_f values affect noise levels, the stationary distributions of mRNAs are simulated at the transcriptional activity of 0.5, where transcriptional activity exhibits the most sensitive response (b and c, star). A slower k_f results in DNA dynamics that are slower relative to mRNA dynamics (i.e., $k_f\Omega^{-1},\ k_r \ll \alpha, \beta$), causing slow transitions between inhibited and activated DNA complexes. These slow transitions between inhibited and activated DNA complexes lead to a bimodal distribution of mRNAs that significantly deviates from the Poisson distribution, leading to a high Fano factor (top). On the other hand, a faster k_f produces unimodal distributions that resemble a Poisson distribution, causing a reduced Fano factor (bottom). (e) Since the relative rates of DNA dynamics (i.e., $k_f\Omega^{-1}$ and k_r) and mRNA dynamics (i.e., α and β) affect noise levels, the Fano factors of mRNA distributions are examined under varying rates. Specifically, the Fano factor at the transcriptional activity of 0.5 is calculated with respect to k_f and the half-life of mRNA ($\ln 2/\beta$), while maintaining the dissociation constant $K_r = k_r/k_f$ and effective transcription rate α/β. When k_f or the half-life is higher and thus k_f becomes faster relative to mRNA dynamics, the Fano factor decreases. However, with biologically realistic k_f and half-life (gray box), noise levels remain substantially high (Fano factor > 45).

https://doi.org/10.1371/journal.pcbi.1013217.g001

that, when the binding rate is sufficiently fast relative to the mRNA half-life ($\ln 2/\beta$), the Fano factor approached its minimal value of 1 (Fig 1e). However, achieving this requires biologically unrealistic fast binding and unbinding rates. Specifically, with a biologically relevant binding rate $k_f\Omega^{-1} = 6 \times 10^{-6} \sim 6 \times 10^{-5}$ $ymol^{-1}min^{-1}$ [24,29,30], where $\Omega = 10^7 aL$ is the volume of the cell [23], and the mRNA half-life is 0.5 ~ 16.4 hours (i.e., 30 ~ 984 min; Table 2) [31,32], the Fano factor is greater than 40 (Fig 1e, gray box). Taken together, while increasing binding rates can minimize noise, the cooperative binding mechanism remains highly noisy under physiological conditions.

Ultrasensitivity generated with indirect repression mechanisms is robust to noise

The transcriptional repression by repressors can occur not only through direct binding to DNA such as cooperative binding mechanism, but also by indirectly inhibiting activators that promote transcription [14,33–36]. In addition, combining multiple indirect repression mechanisms can generate an ultrasensitive transcriptional response [21], while maintaining lower noise levels [22]. Accordingly, we investigated whether the models describing different combinations of indirect repression mechanisms can achieve ultrasensitivity with low transcriptional noise under biologically plausible conditions.

In this model, activators (A) bind to free DNA (E_F) at a rate k_f to form activator-bound DNA (E_A), and unbind at a rate k_a. Once E_A is formed, the transcription is activated, leading to mRNAs production at a rate α and degradation at a rate β (Fig 2a, bottom). To inhibit the transcription, indirect repression mechanisms such as sequestration, blocking, and displacement can be used. Specifically, free repressors (R) can bind to A at a rate k_f, forming an activator-repressor complex (R_A) to prevent A from binding to DNA (sequestration; Fig 2a, top left), while unbinding from R_A at a rate k_s. R can also bind directly to E_A at a rate k_f, forming the activator-repressor-bound DNA (E_R), thereby blocking transcription (blocking; Fig 2a, top middle), while R can unbind from E_R at a rate k_b. Additionally, R removes A from E_R with the form of R_A at a rate k_d, whereas R_A can bind to DNA at a rate k_f reversely (displacement; Fig 2a, top right, and Table 1). Based on these reactions, we constructed three distinct models one with sole sequestration by including only A, R, and R_A dynamics; a second with sequestration and blocking by additionally incorporating R binding/unbinding to E_A; and a third model with all three repressions by further including binding/unbinding between R_A and E_F.

First, by adjusting the dissociation constants $K_s = k_s/k_f$ for sequestration, the model with sequestration alone can achieve ultrasensitivity comparable to that of cooperative binding with four binding sites (Fig 2b, red solid line). Subsequently, adjusting $K_b = k_b/k_f$ for blocking and $K_d = k_d/k_f$ for displacement enables other two models to reach similar levels of ultrasenstivity (Fig 2b, blue and yellow dashed lines). While the level of their ultrasensitivity is similar, interestingly,

Table 1. Propensity functions of reactions and parameter values for all models.

Model	Reaction	Propensity function	Parameter value
The four binding sites model	$E_X \to E_X + M$ $X \in \{0000, 0001, 0010, 0100, 1000, 0011, 0101, 1001, 0110, 1010, 1100, 0111, 1011, 1101, 1110\}$	αn_{E_X}	$\alpha = 100\beta$, $\beta = \frac{\ln 2}{984.5}\ min^{-1}$, $c = 10^{-2}$, $k_f = 600,\ 6 \cdot 10^5\ aL \cdot ymol^{-1} min^{-1}$, $\Omega = 10^7\ aL$, $K_r = 10^{-2}\ ymol$ were used in Fig 1b–1c. $R_T = c^{1.5}\Omega K_r = 100$ was used in Fig 1d.
	$M \to \phi$	βn_M	
	$E_{0000} \to E_X$ $X \in \{0001, 0010, 0100, 1000\}$	$(k_f/\Omega) R_T n_{E_{0000}}$	
	$E_{0001} \to E_X$ $X \in \{0011, 0101, 1001\}$	$(k_f/\Omega) R_T n_{E_{0001}}$	
	$E_{0010} \to E_X$ $X \in \{0011, 0101, 1001\}$	$(k_f/\Omega) R_T n_{E_{0010}}$	
	$E_{0100} \to E_X$ $X \in \{0101, 0110, 1100\}$	$(k_f/\Omega) R_T n_{E_{0100}}$	
	$E_{1000} \to E_X$ $X \in \{1001, 1010, 1100\}$	$(k_f/\Omega) R_T n_{E_{1000}}$	
	$E_{0011} \to E_X$ $X \in \{0111, 1011\}$	$(k_f/\Omega) R_T n_{E_{0011}}$	
	$E_{0101} \to E_X$ $X \in \{0111, 1101\}$	$(k_f/\Omega) R_T n_{E_{0101}}$	
	$E_{1001} \to E_X$ $X \in \{1011, 1101\}$	$(k_f/\Omega) R_T n_{E_{1001}}$	
	$E_{0110} \to E_X$ $X \in \{0111, 1110\}$	$(k_f/\Omega) R_T n_{E_{0110}}$	
	$E_{1010} \to E_X$ $X \in \{1011, 1110\}$	$(k_f/\Omega) R_T n_{E_{1010}}$	
	$E_{1100} \to E_X$ $X \in \{1101, 1110\}$	$(k_f/\Omega) R_T n_{E_{1100}}$	
	$E_{0111} \to E_{1111}$	$(k_f/\Omega) R_T n_{E_{0111}}$	
	$E_{1011} \to E_{1111}$	$(k_f/\Omega) R_T n_{E_{1011}}$	
	$E_{1101} \to E_{1111}$	$(k_f/\Omega) R_T n_{E_{1101}}$	
	$E_{1110} \to E_{1111}$	$(k_f/\Omega) R_T n_{E_{1110}}$	
	$E_X \to E_{0000}$ $X \in \{0001, 0010, 0100, 1000\}$	$k_r n_{E_X}$	
	$E_X \to E_{0001}$ $X \in \{0011, 0101, 1001\}$	$c k_r n_{E_X}$	
	$E_X \to E_{0010}$ $X \in \{0011, 0101, 1001\}$	$c k_r n_{E_X}$	
	$E_X \to E_{0100}$ $X \in \{0101, 0110, 1100\}$	$c k_r n_{E_X}$	
	$E_X \to E_{1000}$ $X \in \{1001, 1010, 1100\}$	$c k_r n_{E_X}$	
	$E_X \to E_{0011}$ $X \in \{0111, 1011\}$	$c^2 k_r n_{E_X}$	
	$E_X \to E_{0101}$ $X \in \{0111, 1101\}$	$c^2 k_r n_{E_X}$	
	$E_X \to E_{1001}$ $X \in \{1011, 1101\}$	$c^2 k_r n_{E_X}$	

(Continued)

Table 1. (Continued)

Model		Reaction	Propensity function	Parameter value
		$E_X \to E_{0110}$ $X \in \{0111, 1110\}$	$c^2 k_r n_{E_X}$	
		$E_X \to E_{1010}$ $X \in \{1011, 1110\}$	$c^2 k_r n_{E_X}$	
		$E_X \to E_{1100}$ $X \in \{1101, 1110\}$	$c^2 k_r n_{E_X}$	
		$E_{1111} \to E_{0111}$	$c^3 k_r n_{E_X}$	
		$E_{1111} \to E_{1011}$	$c^3 k_r n_{E_X}$	
		$E_{1111} \to E_{1101}$	$c^3 k_r n_{E_X}$	
		$E_{1111} \to E_{1110}$	$c^3 k_r n_{E_X}$	
The combination of indirect repressions model	with the sole sequestration	$E_A \to E_A + M$	αn_{E_A}	$\alpha = 100\beta$, $\beta = \frac{\ln 2}{984.5}\ min^{-1}$, $k_f = 600\ aL \cdot ymol^{-1} min^{-1}$, $\Omega = 10^7\ aL$, $A_T = 10^3, 10^4, 10^5$, $\frac{K_s}{A_T} = 4.5 \cdot 10^{-10}\ ymol$, $\frac{K_a}{A_T} = 7 \cdot 10^{-9}\ ymol$, $\frac{K_b}{A_T} = 10^{-6}\ ymol$, $K_d = K_a \cdot K_b / K_s$ were used in Fig 2b–2c. $\frac{K_s}{A_T} = 6 \cdot 10^{-13}\ ymol$, $\frac{K_a}{A_T} = 6 \cdot 10^{-11}\ ymol$, $\frac{K_b}{A_T} = 10^{-6}\ ymol$, $K_d = K_a \cdot K_b / K_s$ were used in Fig 3a–3b.
		$M \to \phi$	βn_M	
		$A + E_F \to E_A$	$(k_f/\Omega)\, A\, (R_T, A_T, K_s)\, n_{E_F}$	
		$E_A \to A + E_F$	$k_a n_{E_A}$	
	with the blocking	$R + E_A \to E_R$	$(k_f/\Omega)\, R\, (R_T, A_T, K_s)\, n_{E_A}$	
		$E_R \to R + E_A$	$k_b n_{E_R}$	
	with the displacement	$R_A + E_F \to E_R$	$(k_f/\Omega)\, R_A\, (R_T, A_T, K_s)\, n_{E_F}$	
		$E_R \to R_A + E_F$	$k_d n_{E_R}$	
The transcriptional NFL model	with the sole sequestration	$E_A \to E_A + M$	αn_{E_A}	$\alpha = 100\beta$, $\beta = \frac{\ln 2}{120}\ min^{-1}$, $\alpha_2 = 5/12\ min^{-1}$, $\alpha_3 = 5/12\ min^{-1}$, $k_f = 600\ aL \cdot ymol^{-1} min^{-1}$, $\frac{K_s}{A_T} = 9 \cdot 10^{-12}\ ymol$, $\frac{K_a}{A_T} = 2 \cdot 10^{-9}\ ymol$, $\frac{K_b}{A_T} = 5 \cdot 10^{-9}\ ymol$, $K_d = K_a \cdot K_b / K_s$ $\Omega = 10^7\ aL$, $A_T = 10^5$, were used in Fig 4g.
		$M \to \phi$	βn_M	
		$M \to R_c$	$\alpha_2 n_M$	
		$R_c \to \phi$	βn_{R_c}	
		$R_c \to R$	αn_{E_A}	
		$R \to \phi$	βn_R	
		$A + E_F \to E_A$	$(k_f/\Omega)\, A\, (R_T, A_T, K_s)\, n_{E_F}$	
		$E_A \to A + E_F$	$k_a n_{E_A}$	
	with the blocking	$R + E_A \to E_R$	$(k_f/\Omega)\, R\, (R_T, A_T, K_s)\, n_{E_A}$	
		$E_R \to R + E_A$	$k_b n_{E_R}$	
	with the displacement	$R_A + E_F \to E_R$	$(k_f/\Omega)\, R_A\, (R_T, A_T, K_s)\, n_{E_F}$	
		$E_R \to R_A + E_F$	$k_d n_{E_R}$	

(Continued)

Table 1. (Continued)

Model		Reaction	Propensity function	Parameter value
The multi-target gene regulation model	with the sole sequestration	$E_A \rightarrow E_A + M$	αn_{E_A}	$\alpha = 100\beta$, $\beta = \frac{\ln 2}{120}\ min^{-1}$, $k_f = 600\ aL \cdot ymol^{-1} min^{-1}$, $K_s = 4.5 \cdot 10^{-10}\ ymol$, $K_a = 7 \cdot 10^{-9}\ ymol$, $K_b = 10^{-6}\ ymol$, $K_d = K_a \cdot K_b / K_s$, $\Omega = 10^7\ aL$, $A_T = 10^3$, $D_T = 0,\ 10,\ 100,\ 1,000,\ 2,000,$ were used in Fig 5b–5d.
		$M \rightarrow \phi$	βn_M	
		$A + E_F \rightarrow E_A$	$(k_f/\Omega)\, n_A n_{E_F}$	
		$E_A \rightarrow A + E_F$	$k_a n_{E_A}$	
		$A + D_F \rightarrow D_A$	$(k_f/\Omega)\, n_A n_{D_F}$	
		$D_A \rightarrow A + D_F$	$k_a n_{D_A}$	
		$R + A \rightarrow R_A$	$(k_f/\Omega)\, n_R n_A$	
		$R_A \rightarrow R + A$	$k_s n_{R_A}$	
	with the blocking	$R + E_A \rightarrow E_R$	$(k_f/\Omega)\, n_R n_{E_A}$	
		$E_R \rightarrow R + E_A$	$k_b n_{E_R}$	
		$R + D_A \rightarrow D_R$	$(k_f/\Omega)\, n_R n_{D_A}$	
		$D_R \rightarrow R + D_A$	$k_b n_{D_R}$	
	with the displacement	$R_A + E_F \rightarrow E_R$	$(k_f/\Omega)\, n_{R_A} n_{E_F}$	
		$E_R \rightarrow R_A + E_F$	$k_d n_{E_R}$	
		$R_A + D_F \rightarrow D_R$	$(k_f/\Omega)\, n_{R_A} n_{D_F}$	
		$D_R \rightarrow R_A + D_F$	$k_d n_{D_R}$	

Here, n_X is the number of X; A_T, R_T, and D_T are the total number of activators, repressors, and additional target genes, respectively. Under the assumption that the binding/unbinding reactions between proteins (i.e., R and A) equilibrate much faster than those between proteins and DNA (i.e., A and E_F, R and E_A, and R_A and E_F), the number of proteins (i.e., R, A, and R_A) equilibrate rapidly and can be approximated by their quasi-steady-state approximations (QSSAs). These are given by:

$A(R_T, A_T, K_s) = \frac{A_T - R_T - \Omega K_s + \sqrt{(A_T - R_T - \Omega K_s)^2 + 4\Omega A_T K_s}}{2}$, $R(R_T, A_T, K_s) = \frac{R_T - A_T - \Omega K_s + \sqrt{(A_T - R_T - \Omega K_s)^2 + 4\Omega A_T K_s}}{2}$, and $R_A(R_T, A_T, K_s) = \frac{A_T + R_T + \Omega K_s - \sqrt{(A_T - R_T - \Omega K_s)^2 + 4\Omega A_T K_s}}{2}$.
This QSSA assumption has been validated through stochastic simulations (S2 Fig).

https://doi.org/10.1371/journal.pcbi.1013217.t001

Table 2. The references of parameter values used for model simulations.

Cell type	Parameter (definition)	Reported range	References
In vitro (Cell host: human NF-κB and IκBα expressed in E. coli BL21 DE3); N/A – Theoretical/ literature-based study; In silico molecular dynamics simulation	k_f (binding rate)	$10^6 \sim 10^7\ M^{-1}s^{-1}$	Williamson, 2023; Bergqvist et al., 2009; Zou et al., 2020
Typical mammalian cells	Ω (cell volume)	$10^{-12} \sim 10^{-11} l$	Milo et al., 2016
Mouse embryonic stem cells, human whole blood	$\ln 2/\beta$ (mRNA half-life)	0.5 (less than 1 h) ∼ 16.4 h	Sharova et al., 2009; Wang & Liu, 2022
H. sapiens cell lines	A_T/Ω (transcription factor concentration)	$10^{-9} \sim 10^{-7} M$	Milo et al., 2016

https://doi.org/10.1371/journal.pcbi.1013217.t002

their noise levels differ (Fig 2c and Table 3). Specifically, as more repression mechanisms are added, the overall noise levels decrease, consistent with a previous study [22].

Next, we investigate whether the noise levels can be further decreased as binding and unbinding rates become faster as shown in cooperative binding. Indeed, as binding rates become faster relative to mRNA half-life, the Fano factor decreases in all three models. However, within the biologically relevant range of binding rate and mRNA half-life, the Fano factor still remains high, with a minimum of about 4 (Table 2 and Fig 2d, top row). In this case, we used the number of activators $A_T = 10^3$. Since the biologically relevant copy number of activators is typically within the range of $A_T = 10^3 \sim 10^5$

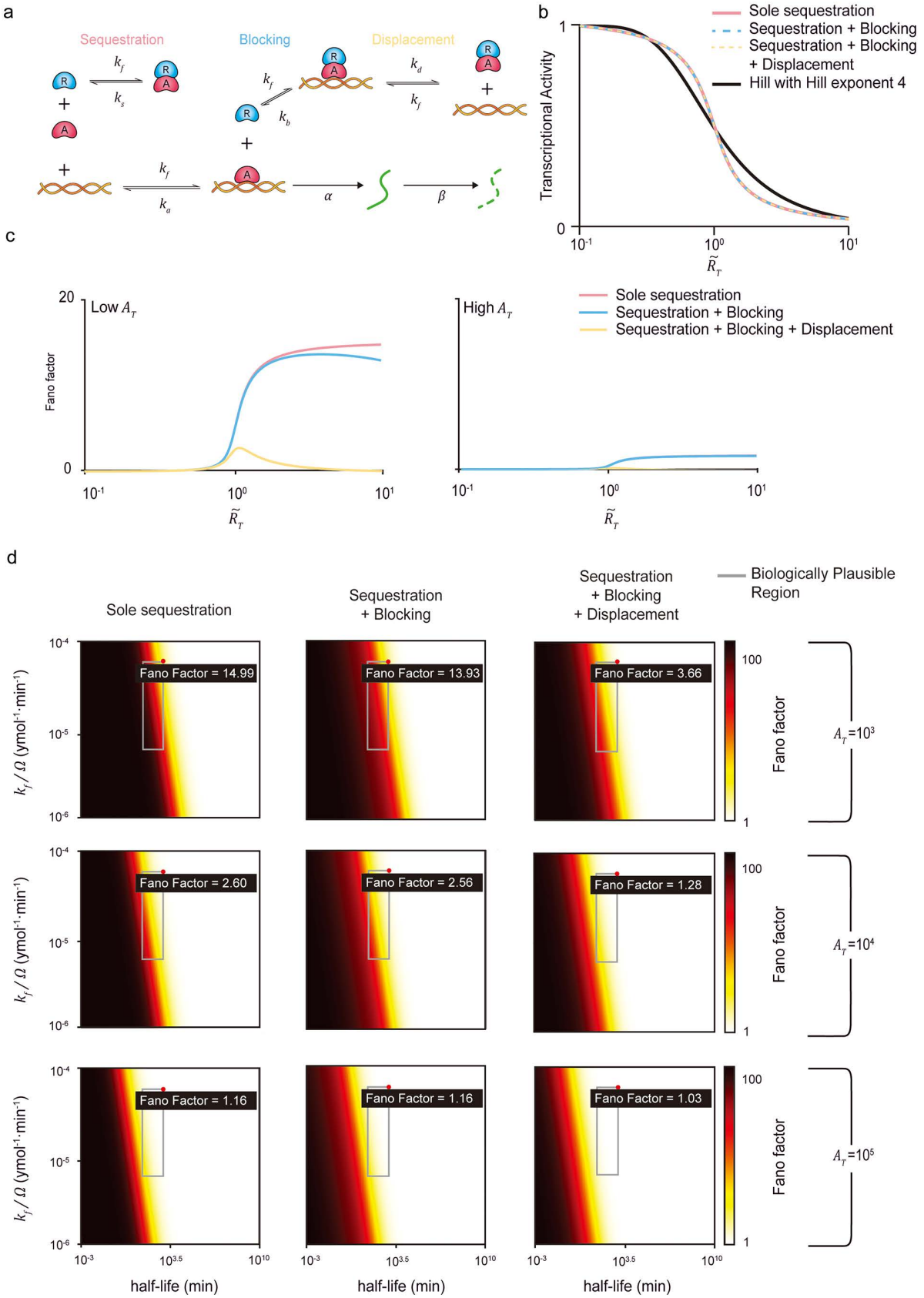
a
Sequestration
Blocking
Displacement
b
Sole sequestration
Sequestration + Blocking
Sequestration + Blocking + Displacement
Hill with Hill exponent 4
Transcriptional Activity
c
Low A_T
High A_T
Fano factor
Sole sequestration
Sequestration + Blocking
Sequestration + Blocking + Displacement
d
Sole sequestration
Sequestration + Blocking
Sequestration + Blocking + Displacement
Biologically Plausible Region
Fano Factor = 14.99
Fano Factor = 13.93
Fano Factor = 3.66
Fano Factor = 2.60
Fano Factor = 2.56
Fano Factor = 1.28
Fano Factor = 1.16
Fano Factor = 1.16
Fano Factor = 1.03
Fano factor
A_T=10^3
A_T=10^4
A_T=10^5
half-life (min)

Fig 2. The combinations of repression mechanisms can achieve minimal noise levels with high sensitivity under biologically realistic conditions. (a) Model diagram of transcription regulated by multiple repression mechanisms. An activator (A) binds to DNA, forming an activated DNA complex (E_A) at a rate k_f, and unbinds from DNA at a rate k_a. Once E_A is formed, mRNAs are produced at a rate α and degrade at a rate β. To prevent the formation of E_A, a repressor (R) sequesters free A at a rate k_f, forming a repressor-activator complex (R_A; sequestration). R also unbinds from R_A at a rate k_s. When A is already bound to DNA, a free R binds directly to the DNA-bound A at a rate k_f forming a repressed DNA complex (E_R; blocking), and unbinds from E_R at a rate k_b. Additionally, free R can displace DNA-bound A from E_R by forming R_A (displacement) at a rate k_d, while R_A binds to DNA at a rate k_f. Accordingly, the dissociation constants are defined as $K_a = k_a/k_f$, $K_s = k_s/k_f$, $K_b = k_b/k_f$, and $K_d = k_d/k_f$. (b) To investigate whether the transcriptional activity of multiple repression mechanisms can exhibit a sensitive response similar to the Hill function, transcriptional activities of the sole sequestration (red solid line), the combination of sequestration and blocking (blue dashed line), and the combination of sequestration, blocking, and displacement (yellow dashed line) are derived. For all three models, when the number of repressors (R_T) is less than the number of activators (A_T), unsequestered activators can bind to DNA, promoting transcription (activation phase). However, when R_T exceeds A_T, most activators are sequestered by repressors, thereby suppressing transcription (repression phase). In the switching from activation to repression phase, a sharp transition occurs when the molar ratio between A_T and R_T ($\widetilde{R_T} = R_T/A_T$) is near one. The sensitivity of this transition is determined by the dissociation constants K_a, K_s, K_b, and K_d; hence, they are appropriately adjusted to match all models that exhibit transcriptional activity comparable to the Hill function with Hill exponent of 4 (black solid line). (c) Despite this similarity in transcriptional activity, the three models show significant differences in overall noise levels. Specifically, overall noise levels decrease with the addition of repression mechanisms: from the sole sequestration (red solid line) to the combination of sequestration and blocking (blue solid line), and further the combination of sequestration, blocking, and displacement (yellow solid line). Additionally, overall noise levels across all $\widetilde{R_T}$ values are lower when A_T is higher (right) compared to when it is lower (left). (d) Given the impact of A_T on overall noise levels across the three models, the Fano factor of mRNAs is examined under varying A_T values. Specifically, the maximum Fano factor near $\widetilde{R_T}$ of 1 is calculated with respect to $k_f\Omega^{-1}$ and the half-life of mRNA, while maintaining the dissociation constant K_a, K_b and K_d, and effective transcription rate α/β. Heatmaps of the maximum Fano factor are shown for the sole sequestration (first column), the combination of sequestration and blocking (second column), and the combination of sequestration, blocking and displacement (third column). Each model is simulated with A_T values of 10^3, 10^4, and 10^5, all of which are biologically realistic. When $A_T = 10^3$(first row), all three models show lower noise levels compared to the cooperative binding model over the same range of $k_f\Omega^{-1}$ and the half-life of mRNA. Furthermore, overall noise levels progressively decrease as the repression mechanisms are added. In particular, within the biologically realistic $k_f\Omega^{-1}$ and the mRNA half-life (gray box), the combination of all three mechanisms reduces the noise level down to the Fano factor of approximately 3, much lower compared to the cooperative binding (i.e., Fano factor = 49). The noise levels are further decreased as the level of A_T increases. When $A_T = 10^5$(third row), the minimum noise levels (i.e., a Fano factor of 1) are achievable within the biologically realistic k_f and the mRNA half-life (gray box) for all three mechanisms.

https://doi.org/10.1371/journal.pcbi.1013217.g002

yoctomole [23], we next tested whether increasing A_T could further suppress noise. Indeed, higher A_T shifted the low noise region towards the biologically realistic parameter space without altering k_f or the mRNA half-life (Fig 2d, middle row). Notably, when A_T was increased to 10^5, in combination with faster binding rates and longer mRNA half-lives, the Fano factor approached ~1 in all three models (Fig 2d, bottom row).

To further investigate noise levels under conditions of higher ultrasensitivity, we adjusted the dissociation constants of the indirect repression mechanisms to produce transcriptional activity with a Hill coefficient of 50 (Fig 3a). This elevated ultrasensitivity is accompanied by increased transcriptional noise (Figs 2c and 3b). This increase amplifies the differences among the models, which originate from stochastic transitions of DNA states (S3 Fig) [22]. Furthermore, such attenuation of transcriptional noise—while maintaining comparable levels of ultrasensitivity through the addition of repression mechanisms—persists even when the numbers of activators and repressors fluctuate due to processes such as repressor birth–death dynamics and repressor-induced activator degradation (S4 Fig). This effect is robust across a broad parameter range, and stronger repression further enhances noise suppression (S5 Fig). Accordingly, under biologically relevant conditions, only the combination of sequestration, blocking, and displacement exhibits a low Fano factor ranging from 1 to 20—consistent with the experimentally observed range in mammalian cells—and is uniquely capable of reducing it to values close to 1 [37] (Fig 3c).

Multiple biological oscillators employ a combination of sequestration, blocking, and displacement mechanisms to produce rhythms that are both robust and precise

The combination of sequestration, blocking, and displacement constitutes a core regulatory logic shared across diverse biological oscillators. In the mammalian circadian clock, the PER-CRY complex sequesters CLOCK-BMAL1, displaces it from DNA, and CRY further blocks its transcriptional activity [21,38–44] (Fig 4a). In the NF-κB oscillator, IκB sequesters NF-κB in the cytoplasm, and upon external stimulation, its degradation allows NF-κB to activate transcription; this

Table 3. The transcriptional activity and the Fano factor for all models describing combinations of indirect repression mechanisms.

The sequestration-based switch	Transcriptional activity	$\frac{A(R_T,A_T,K_s)/\Omega K_a}{1+A(R_T,A_T,K_s)/\Omega K_a}$ where $A(R_T,A_T,K_s)=\frac{A_T-R_T-\Omega K_s+\sqrt{(A_T-R_T-\Omega K_s)^2+4\Omega A_T K_s}}{2}$.
	Fano factor	$1+\frac{\alpha}{k_f(1+A(R_T,A_T,K_s)/\Omega K_a)(A(R_T,A_T,K_s)/\Omega+K_a+\beta/k_f)}$
The sequestration- and blocking-based switch	Transcriptional activity	$\frac{\frac{A(R_T,A_T,K_s)}{\Omega K_a}}{1+\frac{A(R_T,A_T,K_s)}{\Omega K_a}+\frac{A(R_T,A_T,K_s)}{\Omega K_a}\frac{R(R_T,A_T,K_s)}{\Omega K_b}}$ where $R(R_T,A_T,K_s)=\frac{R_T-A_T-\Omega K_s+\sqrt{(A_T-R_T-\Omega K_s)^2+4\Omega A_T K_s}}{2}$.
	Fano factor	$1+\frac{\alpha\left[K_b+\frac{\beta}{k_f}+\left(\frac{A(R_T,A_T,K_s)}{\Omega}+\frac{\beta}{k_f}\right)\frac{A(R_T,A_T,K_s)}{\Omega K_a}\frac{R(R_T,A_T,K_s)}{\Omega K_b}\right]}{k_f\left(1+\frac{A(R_T,A_T,K_s)}{\Omega K_a}+\frac{A(R_T,A_T,K_s)}{\Omega K_a}\frac{R(R_T,A_T,K_s)}{\Omega K_b}\right)\left[K_a\left(K_b+\frac{\beta}{k_f}\right)+\left(\frac{A(R_T,A_T,K_s)}{\Omega}+\frac{\beta}{k_f}\right)\left(\frac{R(R_T,A_T,K_s)}{\Omega}+K_b+\frac{\beta}{k_f}\right)\right]}$
The sequestration-, blocking- and displacement-based switch	Transcriptional activity	$\frac{I(R_T,A_T,K_a,K_s)\frac{A(R_T,A_T,K_s)}{\Omega K_a}}{1+I(R_T,A_T,K_a,K_s)\frac{A(R_T,A_T,K_s)}{\Omega K_a}+J(R_T,A_T,K_a,K_s)\frac{A(R_T,A_T,K_s)}{\Omega K_a}\frac{R(R_T,A_T,K_s)}{\Omega K_b}}$ where $I(R_T,A_T,K_a,K_s)=\frac{K_s+\sigma K_a+R(R_T,A_T,K_s)/\Omega}{K_s+\sigma K_a+\sigma R(R_T,A_T,K_s)/\Omega}$, $J(R_T,A_T,K_a,K_s)=\frac{K_s+K_a+R(R_T,A_T,K_s)/\Omega}{K_s+\sigma K_a+\sigma R(R_T,A_T,K_s)/\Omega}$, and $\sigma=\frac{K_s K_d}{K_a K_b}$.
	Fano factor	$1+\frac{\alpha\left[\left(\frac{R_A(R_T,A_T,K_s)}{\Omega}+K_b+K_d+\frac{\beta}{k_f}\right)+\left(\frac{A_T}{\Omega}+K_d+\frac{\beta}{k_f}\right)J(R_T,A_T,K_a,K_s)\frac{A(R_T,A_T,K_s)}{\Omega K_a}\frac{R(R_T,A_T,K_s)}{\Omega K_b}\right]}{k_f\left(1+I(R_T,A_T,K_a,K_s)\frac{A(R_T,A_T,K_s)}{\Omega K_a}+J(R_T,A_T,K_a,K_s)\frac{A(R_T,A_T,K_s)}{\Omega K_a}\frac{R(R_T,A_T,K_s)}{\Omega K_b}\right)\left[\left(K_b+K_d+\frac{\beta}{k_f}\right)\left(\frac{A(R_T,A_T,K_s)}{\Omega}+K_d+\frac{\beta}{k_f}\right)+\left(K_b+K_a+\frac{\beta}{k_f}\right)\frac{R_A(R_T,A_T,K_s)}{\Omega}+\left(\frac{A_T}{\Omega}+K_d+\frac{\beta}{k_f}\right)\frac{R(R_T,A_T,K_s)}{\Omega}\right]}$, where $R_A(R_T,A_T,K_s)=\frac{A_T+R_T+\Omega K_s-\sqrt{(A_T-R_T-\Omega K_s)^2+4\Omega A_T K_s}}{2}$.

https://doi.org/10.1371/journal.pcbi.1013217.t003

activation is subsequently suppressed as IκB displaces NF-κB from the DNA [29,45] (Fig 4b). In the p53-Mdm2 oscillator, Mdm2 sequesters p53 away from DNA, blocks transcriptional activity of p53, and displaces it from DNA through cooperative interactions with other corepressors [46,47] (Fig 4c). Although these systems differ in their biological roles—circadian rhythms must sustain precise oscillations under constant conditions, whereas NF-κB and p53 oscillations are transient and stimulus-induced—they employ the same regulatory strategy to achieve functional robustness. The coordinated action of sequestration, blocking, and displacement sharpens the input–output response, creating ultrasensitivity while buffering against fluctuations in upstream signals. We hypothesized that this noise-resistant ultrasensitive switch (Fig 4d, left) enables strong oscillatory responses and precise timing of transitions between transcriptional on and off states (Fig 4d, right) [1,3,4,14], thereby ensuring coherent and stable oscillations once they are triggered.

To validate this hypothesis, we constructed a transcriptional negative feedback loop (NFL) model (Fig 4e and Table 1). In the NFL model, transcriptional activation leads to the synthesis of mRNA (M), which is subsequently translated into the repressor in the cytoplasm (R_c). Upon nuclear entry, the repressor (R) suppresses its own transcription via multiple

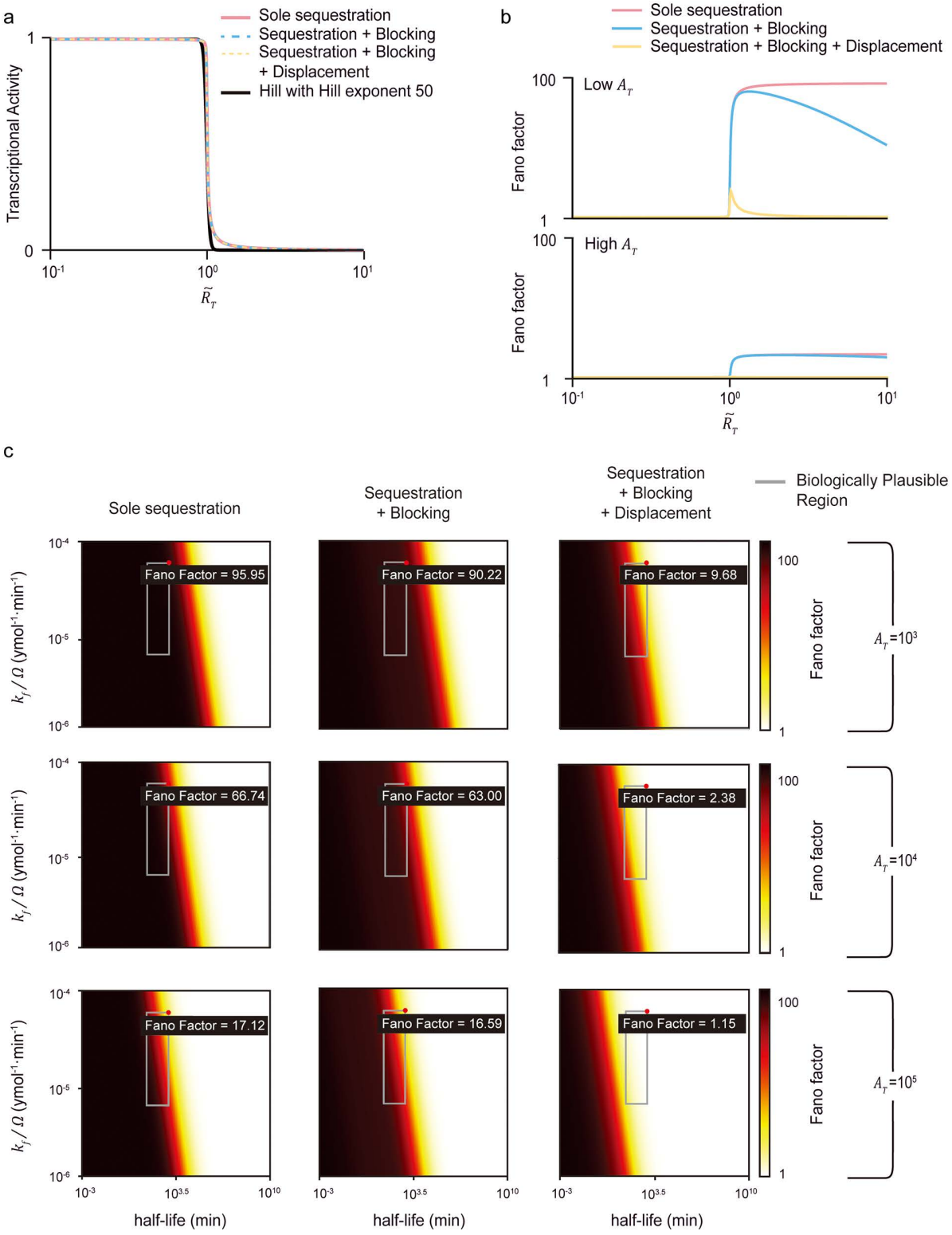

Fig 3. Only the combination of sequestration, blocking and displacement can achieve close to the minimum noise levels with considerably high sensitivity under biologically realistic conditions. (a) The transcriptional activities of the sole sequestration (red solid line), the combination of sequestration and blocking (blue dashed line), and the combination of sequestration, blocking, and displacement (yellow dashed line) are matched to

resemble the Hill function with Hill exponent of 50 (black solid line) by adjusting the dissociation constants K_a, K_s, K_b, and $\mathbf{K}_d$. (b) Despite similarities in transcriptional activities, the three models show significant differences in overall noise levels (top). These noise levels decrease with the addition of repression mechanisms, from the sole sequestration (red solid line) to the combination of sequestration and blocking (blue solid line), and further to the combination of sequestration, blocking, and displacement (yellow solid line). Notably, more sensitive responses with Hill exponent of 50 induce greater noise levels compared to those observed with Hill exponent of 4 (Fig 2c, top). Furthermore, increasing A_T leads to an overall reduction in noise levels (bottom). (c) The maximum Fano factor for each model under varying A_T values is shown. When $A_T = 10^3$ (first row), all models show high noise levels (i.e., Fano factor > 9) over the biological range of $k_f\Omega^{-1}$ and the mRNA half-life. Noise levels decrease as A_T increases (2nd and 3rd rows). In particular, when $A_T = 10^5$, the combination of all three mechanisms can lead to reduced noise levels (i.e., a Fano factor close to 1). On the other hand, sole sequestration still results in considerable noise levels (i.e., Fano factor = 17).

https://doi.org/10.1371/journal.pcbi.1013217.g003

repression mechanisms (Fig 4e, gray box). Using this model, we simulated a time-series of mRNA copy numbers ($M(t)$) to investigate the robustness of each repression mechanism against noise (Fig 4f, top). Specifically, we calculated autocorrelation functions of 300 simulated $M(t)$ ($C(t)$; Fig 4f, bottom, green solid line), and fitted them to a decaying cosine function, $\widetilde{C}(t) = e^{-t/\tau} \cdot \cos\frac{2\pi t}{T}$, to estimate T and τ (Fig 4f, bottom, gray dashed line). By definition of $\widetilde{C}(t)$, T represents the period of the rhythm, while τ reflects how slowly the autocorrelation decays [48,49]. We observed that, as additional repression mechanisms were incorporated, the variance in the estimated T decreased. It implies more consistent periods in each cycle of rhythm under noise (Fig 4g), indicating enhanced robustness to noise.

The combination of indirect repressions preserves noise robustness even under multi-target gene regulation

We analyzed models in which 1,000–100,000 transcriptional activators regulate a single target gene (Fig 2a). However, in many biological systems employing multiple repression mechanisms—such as the circadian clock, NF-κB oscillator, and p53-Mdm2 oscillator (Fig 4a–4c)—transcriptional activators often regulate hundreds to thousands of genes simultaneously (Fig 5a). For example, in the mammalian circadian clock, a limited pool of BMAL1 proteins regulates approximately 3,400 genes [50]; p53 controls around 3,700 target genes [51]; and NF-κB targets several hundred genes [52].

Previous studies have suggested that such shared regulation can increase noise, as multiple target genes compete for a limited pool of transcriptional activators [53,54]. To examine whether our proposed mechanisms can overcome this effect, we extended each indirect repression model to include varying numbers of target genes, with regulation mediated through the corresponding repression mechanisms (Fig 5a and Table 1). Notably, increasing the number of target genes has a similar effect as increasing the number of repressors, as it reduces transcriptional activity for the same number of repressors. Thus, for fair comparisons, we evaluated the noise level of each model at equivalent levels of transcriptional activity rather than with equal numbers of repressors (Fig 5b–5d).

Surprisingly, we found that the combination of three indirect repressions preserves noise robustness even under multi-target gene regulation. When the number of the target genes was smaller than that of activators (i.e., 1,000), the transcriptional noise of individual genes remained largely unaffected (Fig 5b–5d, Target gene 0, 10, and 100). Specifically, regardless of repression via the sole sequestration (Fig 5b), the combination of sequestration and blocking (Fig 5c), or the combination of sequestration, blocking, and displacement (Fig 5d), the Fano factor for multiple targets closely matched those of single-target regulation (gray dashed lines). In contrast, when the number of target genes exceeded that of activators (Fig 5b–5d, Target gene 1,000, and 2,000), the Fano factor slightly deviated from the single-target case in the full combination model (Fig 5d), but not in the others (Fig 5b and 5c). This deviation arose because, in the absence of repressors, multiple target genes indirectly suppressed each other by depleting the available activator pool (Fig 5d, red-circled points). This competition effectively acts as an additional layer of sequestration, even in the combined repression model, increasing the noise to a level comparable to that of the sole sequestration model. However, as the number of repressors increased (i.e., as the transcriptional activity decreased), the multiple repression effects became dominant. Consequently, the Fano factor converged to that of the single-target case with multiple repressions (Fig 5d). These results indicate that, contrary to the conventional expectation that multi-target regulation amplifies transcriptional noise, the combined

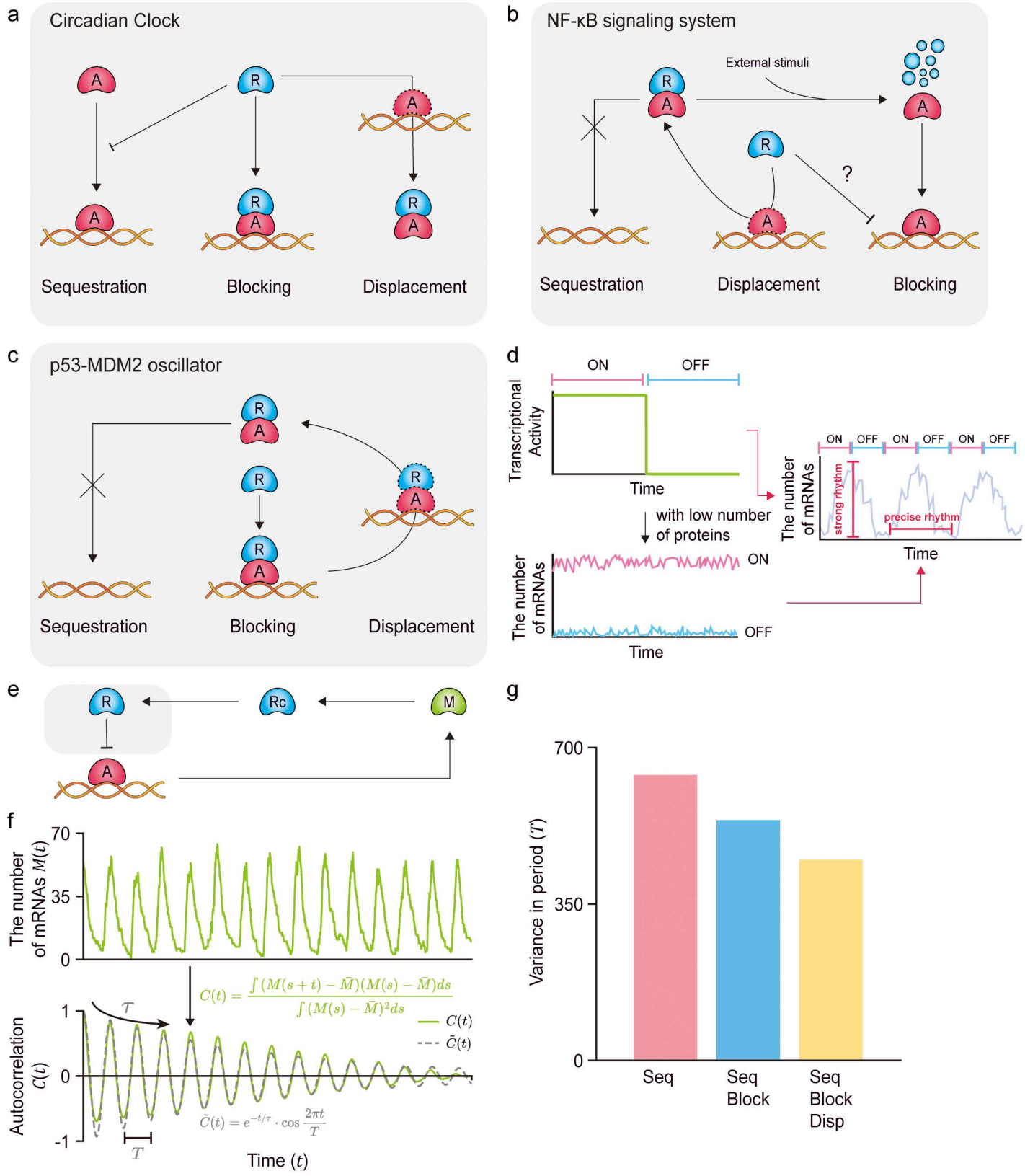

Fig 4. Various biological oscillators utilize the combination of sequestration, blocking, and displacement mechanisms to generate robust and precise rhythms. (a) In the mammalian circadian clock, PER:CRY inhibits CLOCK:BMAL1 by sequestration, preventing its binding to DNA. On the

other hand, when CLOCK:BMAL1 is already bound to DNA, CRY blocks transcription or PER:CRY can displace it from DNA. (b) In the NF-κB signaling system, IκB sequesters NF-κB in the cytoplasm, preventing its entry into the nucleus. As IκB degrades in response to external stimuli, the previously sequestered NF-κB is released and enters the nucleus. In the nucleus, NF-κB binds to DNA to promote transcription. IκB can inhibit transcription by displacing NF-κB from DNA, although whether IκB can directly block transcription remains unclear. (c) In the p53-MDM2 oscillator, MDM2 binds to p53, preventing its binding to DNA. On the other hand, when p53 is already bound to DNA, MDM2 inhibits transcription by directly binding to the DNA-bound p53 to block it, as well as displacing it from DNA in cooperation with a corepressor. (d) The combination of sequestration, blocking, and displacement can generate both high sensitivity and robustness against noise, essential for strong and precise rhythms, respectively. Furthermore, even with a low number of proteins (i.e., activators and repressors), mRNAs exhibit low fluctuations in both on and off transcriptional states. Consequently, biological oscillators incorporating all three mechanisms can effectively produce precise rhythms, with accurate increases and decreases during the transcriptional on and off states, respectively. (e) To investigate this, we constructed the transcriptional negative feedback loop (NFL) model. In the NFL model, when the transcription is turned on, mRNA (M) is produced, and subsequently translated into the cytoplasmic repressor (R_c). After entering the nucleus, the nucleic repressor (R) inhibits its own transcription through the multiple repression mechanisms (gray box). (f) Using the NFL model, the oscillatory time-series of mRNA copy numbers ($M(t)$) can be simulated (top). To quantify the noise level in $M(t)$, its autocorrelation function $C(t)$ (bottom, green solid line) is computed and is fitted with a decaying cosine function $\tilde{C}(t) = e^{-t/\tau} \cdot \cos\frac{2\pi t}{T}$ (bottom, gray dashed line). Here, T represents the period of oscillation, and τ represents how slow $C(t)$ decays. (g) By simulating $M(t)$ for three models over 300 times, we evaluated the variance of T. As more repression mechanisms are combined, the variance of T is reduced, indicating enhanced robustness against noise.

https://doi.org/10.1371/journal.pcbi.1013217.g004

sequestration, blocking, and displacement mechanisms can buffer against such fluctuations, enabling a finite pool of activators to robustly regulate large gene networks.

Discussion

Previous work demonstrated that combining indirect repression mechanisms—such as sequestration, blocking, and displacement—can generate ultrasensitive transcriptional switches that are more robust to molecular noise than direct mechanisms such as cooperative binding [22]. However, those studies did not account for the timescales of DNA-binding dynamics (i.e., the binding and unbinding rates between DNA and transcriptional factors). Here, we show that this omission can be misleading: when DNA binding occurs on a faster timescale than mRNA-related processes (i.e., transcription and degradation), ultrasensitivity and noise robustness can be simultaneously achieved in the resulting transcriptional switch (Fig 1b–1e, 2b, and d), regardless of the underlying repression mechanism. We further show that increasing the number of activators can also promote such ultrasensitive behavior (Fig 2b–2d). However, under realistic constraints on binding kinetics and activator abundance, robust ultrasensitive switching is only achieved when all three indirect repression mechanisms are combined (Fig 3). As a result, biological oscillators incorporating this triple-repression architecture can maintain precise rhythmic transitions between transcriptional states even in the presence of molecular noise (Fig 4). In summary, our findings suggest that combining indirect repression mechanisms offers a resource-efficient strategy for achieving robust, rhythmic gene expression in noisy cellular environments—potentially explaining why sequestration, blocking, and displacement often co-occur in natural biological oscillators.

This strategy is exemplified in systems such as NF-κB oscillators, which often exhibit heterogeneous single-cell oscillatory responses [55]. This heterogeneity primarily results from differences in upstream stimulus strength or duration, such as variations in inflammatory stimuli TNF-α pulse strength or duration that modulate the timing of NF-κB activation [56]. Similarly, in the p53-MDM2 oscillators, cell-to-cell variability in oscillatory dynamics is induced by differences in DNA damage or oncogenic stress [57]. These demonstrate that variability in input stimuli primarily determines when and how cells cross the activation threshold, required to initiate oscillations [58,59]. Therefore, our findings are primarily relevant to the regime where oscillations are triggered by sufficiently strong inputs, and to how the identified repression mechanisms help maintain coherent and stable rhythms of initiated oscillations. Extending this framework to variable input conditions, where upstream stimuli couple with repression strategies thus presents a compelling future research direction for understanding population-level transcriptional dynamics.

Although multiple indirect repression mechanisms may help improve population-level coherence and enhance noise resilience, these advantages could come at a cost at the single-cell level, particularly when compared with direct

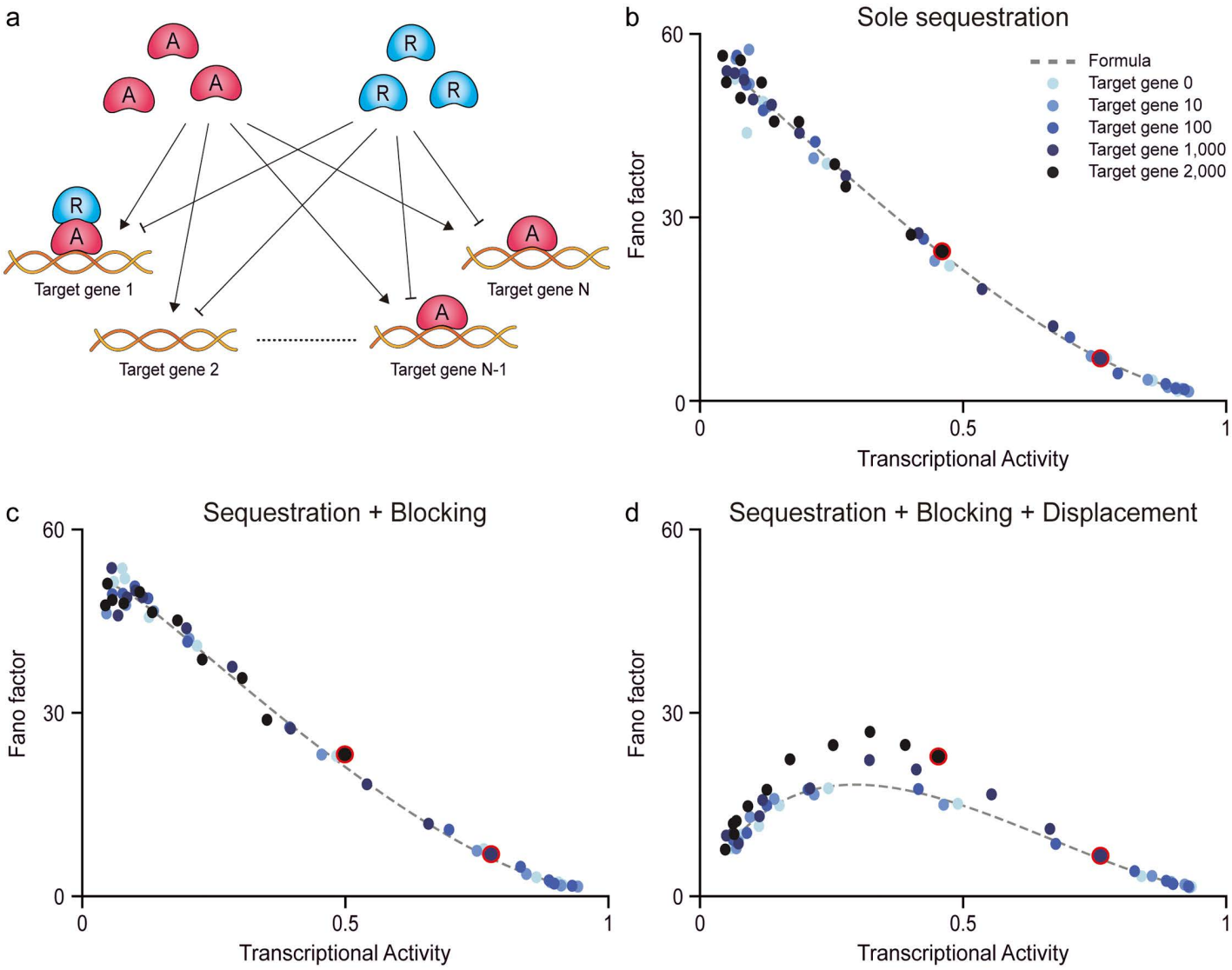

Fig 5. Transcriptional factors regulate thousands of target genes while maintaining noise levels comparable to those of single-gene regulation, given the same level of transcriptional activity. (a) In biological systems, transcriptional activators and repressors often regulate multiple target genes simultaneously. (b–d) We examine whether combining different repression mechanisms can still reduce transcriptional noise. For this, we simulated the stationary distribution of mRNA of one target gene while varying the number of additional target genes to 0, 10, 100, 1,000, and 2,000 (see Methods). From the distribution, we calculated the Fano factor of mRNAs (blue dots). Regardless of the number of target genes, repression via the sole sequestration (b), the combination of sequestration, and blocking (c), the combination of sequestration, blocking, and displacement (d), all show transcriptional noise levels similar to single-gene regulation. Here, dashed lines represent the relationship between the transcriptional activity and the Fano factor without additional target genes.

https://doi.org/10.1371/journal.pcbi.1013217.g005

repressor–DNA binding. Specifically, indirect repression mechanisms inherently require the production of additional proteins (i.e., activators), thereby imposing higher energetic and biosynthetic demands on the cell. The synthesis and maintenance of these additional proteins consume substantial biosynthetic resources, and they can limit the cell's capability to produce other essential proteins, which the cell requires to function properly [60–62]. As a result, it is plausible that natural selection often favors simpler regulatory strategies such as direct repressor-DNA binding, which provide efficient

transcriptional control with lower biosynthetic cost, even if this comes at the cost of reduced noise resilience and ultrasensitivity. This may explain why many biological systems have evolved to select a direct repressor-DNA binding mechanism [63]. Overall, this trade-off between functional performance and resource limitation may represent a fundamental design principle in transcriptional regulation, and investigating how cells balance these competing demands offers a promising avenue for future research.

Indeed, recent studies have shown that consuming resources, i.e., energy, can enhance functional performance, including ultrasensitivity and noise-resilience, in biological oscillators. For example, we show that, without energy consumption (i.e., under the detailed balance condition $\frac{K_a K_b}{K_s K_d} = 1$) [21], simply combining indirect repression mechanisms can enhance the noise robustness of biological oscillators (Fig 4). However, recent studies suggest that breaking detailed balance through energy dissipation can further amplify ultrasensitivity. For example, Jeong et al. demonstrated that violating detailed balance in triple-mechanism models yields greater ultrasensitivity than in other combinations [21]. Similarly, Estrada et al. showed that in cooperative binding systems, breaking detailed balance facilitates ultrasensitive responses [64]. Moreover, energy consumption has also been linked to enhanced noise robustness in oscillatory systems: Cao et al. theoretically showed that energy dissipation suppresses phase diffusion due to intrinsic noise in various biochemical oscillators [49], while Fei et al., using the Brusselator model, found that energy expenditure not only reduces phase diffusion but also improves adaptability to environmental changes [65]. Collectively, these findings highlight that beyond combining repression mechanisms, the energy cost of regulatory processes plays a key role in tuning ultrasensitivity and robustness. Investigating how energy dissipation interacts with transcriptional repression strategies thus presents another compelling direction for future research.

Beyond transcriptional repression, several non-transcriptional mechanisms have also been shown to generate ultrasensitive responses in biological systems. For instance, multisite binding without cooperativity can produce ultrasensitivity when coupled with other processes such as differential degradation or modification rates among molecular complexes [66,67]. Similarly, post-transcriptional regulation through microRNA-mediated repression or RNA-binding proteins can give rise to threshold-like responses and tune gene expression sensitivity [68,69]. At the post-translational level, protein modification cycles—such as phosphorylation–dephosphorylation cascades or ubiquitination [15,16,19]—can further amplify response sensitivity and fine-tune the dynamic range through mechanisms such as enzyme saturation [2,70]. Therefore, investigating how these non-transcriptional mechanisms operating at translational, post-transcriptional, and post-translational levels influence transcriptional noise would be an interesting direction for future research.

Finally, we derived analytical expressions for the mean (i.e., transcriptional activity) and the Fano factor of mRNA across different repression models. While our analysis focused on these stationary statistics, recent analytical advances suggest that more detailed stochastic quantities can also be obtained. Specifically, by applying multiscale simplification techniques [71], the full probability distribution of mRNA for the multi–binding-site model (Fig 1a) could in principle be derived. Similarly, the autocorrelation function of the oscillator model, which we used to characterize noisy rhythmic properties in biological oscillators (Fig 4), could be derived using linear noise approximation [72]. Extending our framework in these directions would deepen understanding of the stochastic underpinnings of gene regulation and provide additional validation for the theoretical conclusions drawn here.

Methods

Derivation of the equations for the transcriptional activity and the Fano factor of the four binding sites model with cooperative binding

To derive the transcriptional activity and Fano factor of a gene regulated by cooperative binding at four DNA sites, we followed the framework introduced by Sanchez et al. [28], formulating a chemical master equation (CME) that captures all 16 possible DNA binding configurations. By computing steady-state moment equations for mRNA distributions, we obtained closed-form expressions for the transcriptional activity and Fano factor as functions of repressor concentration

and binding parameters. These derivations quantify how cooperative repression influences gene expression dynamics, and the full mathematical details are provided in the Supplementary Information and at https://github.com/Mathbiomed/Ultrasensitive-gene-switch.

Derivation of the equations for the transcriptional activity and the Fano factor of the multiple indirect repression mechanism models

Following the approach in the previous section, Jeong et al., derived equations for the transcriptional activity and the Fano factor in models incorporating the multiple indirect repression models [22]. Notably, for analytical convenience, all parameters were normalized by $\left(k_f\Omega^{-1}\right) A_T$. For example, under this normalization, the transcription and degradation rates of mRNA, α and β, were simply switched to $\widetilde{\alpha} = \alpha\Omega/k_f A_T$ and $\widetilde{\beta} = \beta\Omega/k_f A_T$, respectively, and the unbinding rate between activators and DNA, k_a, was expressed as the normalized dissociation constant, $\widetilde{K_a} = \Omega K_a/A_T$. In particular, the binding of activators $\left(k_f\Omega^{-1}\right) A\left(R_T, A_T, K_s\right)$, where the number of free activators is given by

$$A\left(R_T, A_T, K_s\right) = \frac{A_T - R_T - \Omega K_s + \sqrt{\left(A_T - R_T - \Omega K_s\right)^2 + 4\Omega A_T K_s}}{2},$$

was normalized to the fraction of free activators among the total activators,

$$\widetilde{A}\left(\widetilde{R_T}, \widetilde{K_s}\right) = \frac{A\left(R_T, A_T, K_s\right)}{A_T} = \frac{1 - \widetilde{R_T} - \widetilde{K_s} + \sqrt{\left(1 - \widetilde{R_T} - \widetilde{K_s}\right)^2 + 4\widetilde{K_s}}}{2}$$

where $\widetilde{R_T} = R_T/A_T$ and $\widetilde{K_s} = \Omega K_s/A_T$ [14,22,35,73–76]. With the normalized variables and parameters, the transcriptional activity and the Fano factor for the sole sequestration model were derived as follows:

$$TA\left(\widetilde{R_T}\right) = \frac{\widetilde{A}\left(\widetilde{R_T}, \widetilde{K_s}\right)/\widetilde{K_a}}{1 + \widetilde{A}\left(\widetilde{R_T}, \widetilde{K_s}\right)/\widetilde{K_a}},$$

$$FF\left(\widetilde{R_T}\right) = 1 + \frac{\widetilde{\alpha}}{\left(1 + \widetilde{A}\left(\widetilde{R_T}, \widetilde{K_s}\right)/\widetilde{K_a}\right)\left(\widetilde{A}\left(\widetilde{R_T}, \widetilde{K_s}\right) + \widetilde{K_a} + \widetilde{\beta}\right)}.$$

To incorporate k_f, A_T, and Ω to the equations explicitly, we substitute $\widetilde{\alpha}$, $\widetilde{\beta}$, $\widetilde{R_T}$, $\widetilde{K_a}$, and $\widetilde{K_s}$ with the original parameters as follows:

$$TA\left(R_T\right) = \frac{A\left(R_T, A_T, K_s\right)/\Omega K_a}{1 + A\left(R_T, A_T, K_s\right)/\Omega K_a},$$

$$FF\left(R_T\right) = 1 + \frac{\alpha}{k_f\left(1 + A\left(R_T, A_T, K_s\right)/\Omega K_a\right)\left(A\left(R_T, A_T, K_s\right)/\Omega + K_a + \beta/k_f\right)}.$$

Similarly, we substituted the original parameters into the transcriptional activity and the Fano factor equations derived in Jeong et al for other combinations of indirect repression mechanisms (Table 3).

Simulations of multi-target genes regulation and noise level quantification

To evaluate how transcriptional noise is affected when transcriptional activators regulate multiple target genes, we extended the multiple indirect repression models to include up to 2,000 co-regulated genes (Fig 5). To isolate the effect of multi-gene regulation, we fixed the total number of activators to 1,000, while the number of additional target genes was varied from 0 to 2,000. For each gene count, we modulated the transcriptional activity by varying the number of repressors from 0 to 2,000. For each parameter set, we simulated the corresponding CME (Table 1) using the Gillespie algorithm with 1,000 independent runs. The transcriptional activity (i.e., the probability that the gene is active) was quantified as the proportion of runs in which $E_A = 1$ at the stationarity (Fig 5b–5d, x-axis). Similarly, from resulting stationary mRNA distributions, we calculated the Fano factor to measure the transcriptional noise (Fig 5b–5d, y-axis).

Supporting information

S1 Text. Derivation of the equations for the transcriptional activity and the Fano factor of the four binding sites model with cooperative binding.
(DOCX)

S1 Fig. The cooperative binding mechanism, in which activator binding activates transcription, is sensitive to noise. (a) Model diagram of the transcription regulated by the activator proteins (A) binding to four independent sites on the DNA within a cell volume of Ω. Each binding site is occupied by A at a rate k_f. Conversely, A unbinds from DNA at a rate k_a when one site is occupied, with the dissociation constant between A and DNA defined as $K_a = \frac{k_a}{k_f}$. For two, three, or four occupied sites, A unbinds at rates ck_a, c^2k_a and c^3k_a, respectively. Accordingly, when $c < 1$, cooperative binding is present. When all binding sites are occupied, mRNA is produced at a rate α and degrades at a rate β, whereas transcription is inactive if any site remains unoccupied. (b) When $c = 10^{-2}$, transcriptional activity closely resembles the Hill function with a Hill exponent of 4 (black line). Furthermore, transcriptional activity remains consistent with the Hill function regardless of k_f values, provided K_a is kept constant (red dotted line and blue dashed line). (c) Nevertheless, the overall noise level quantified by the Fano factor of mRNAs shows significant differences based on k_f. Notably, the overall noise levels are reduced during the sensitive response when k_f is faster (red solid line) compared to when it is slower (blue solid line).
(TIF)

S2 Fig. The original parameter set does not fully satisfy the conditions required for the quasi–steady-state approximation (QSSA). (a) Ten representative time-series of mRNA copy numbers (thin lines) and their mean trajectories (thick lines) were obtained from 1,000 stochastic simulations using the model that combines sequestration, blocking, and displacement. The reduced model, in which the numbers of activators and repressors are approximated by their QSSA (gray lines; see Methods), was compared with the full model that explicitly models the binding and unbinding reactions between them (green lines). Simulations were performed while varying the molar ratio $\widetilde{R_T} = 0.2$ (left), 1 (middle), and 5 (right), with the original parameter set in Table 1. (b) Probability density functions of the simulated mRNA copy numbers at 500 h, obtained from 1,000 stochastic simulation runs varying the molar ratio $\widetilde{R_T} = 0.2$ (left), 1 (middle), and 5 (right). The full and reduced models show consistent dynamics at each $\widetilde{R_T}$.
(TIF)

S3 Fig. Simulated time-series of DNA states and mRNA copy numbers, and stationary distribution of mRNA copy numbers across the three repression models. (a–c) Stationary distributions of mRNA copy numbers for the sole sequestration (a), combined sequestration and blocking (b), and combined sequestration, blocking, and displacement models (c), simulated using the parameters in Fig 3 at $\widetilde{R_T} = 5$. Despite the large number of repressors compared to the activators, both the sole sequestration model and the combined sequestration and blocking model exhibited bimodal

mRNA distributions, with peaks at both low and high mRNA numbers, indicating that the activated DNA state persisted even in the presence of many repressors. In contrast, incorporation of displacement rendered the mRNA distribution unimodal, reflecting more consistent transcriptional repression. (d-i) Even under a large excess of repressors over activators, the sequestered activator can stochastically dissociate and rebind to DNA to form the active complex E_A (d–f(i), at time 0). In the sole sequestration model (d), once the activator binds to DNA to form E_A (d(i)), it remains bound for a long duration before dissociating into E_F (d(ii)). This leads to continuous mRNA accumulation (g), and thus a bimodal mRNA distribution with a high Fano factor. In the combined sequestration and blocking model (e), E_A rapidly transitions to the repressed state E_R via blocking (e(i) and (ii)), and frequently interconverts between E_A and E_R until the activator dissociates from DNA to form E_F (e(iii)). These frequent blocking events delay mRNA accumulation (h), and reduce the separation between the two peaks in the mRNA distribution, resulting in a lower Fano factor than in the sole sequestration model. In contrast, in the combined sequestration, blocking, and displacement model (f), E_A rapidly transitions to E_R (f(i) and (f(ii))) and displacement accelerates the transition from E_R to E_F (f(iii)), thereby preventing mRNA accumulation (i) and producing a unimodal mRNA distribution with a low Fano factor.
(TIF)

S4 Fig. Despite fluctuations in repressor or activator copy number, the combined sequestration, blocking, and displacement model maintains robustness of noise reduction. (a) When a repressor is regulated by a simple birth–death process, its copy number (R_T) follows a Poisson distribution with the mean of $< R_T >$. (b) In this case, the total mean of the mRNA copy number (M) can be calculated through the law of the total mean, $E[M] = E_\pi\left[E\left[M|R_T\right]\right]$, where denotes the probability mass function of Poisson distribution with the mean of $< R_T >$ and $E\left[M|R_T\right]$ is the conditional mean of M for a given R_T. As $E_\pi\left[E\left[M|R_T\right]\right]$ can be calculated as the product of the production-to-degradation rate ratio (α/β) and the transcriptional activity $TA\left(R_T\right)$ in Table 2 (i.e., $E\left[M|R_T\right] = \frac{\alpha}{\beta} TA\left(R_T\right)$), the total mean of M becomes $E[M] = E_\pi\left[\frac{\alpha}{\beta} TA\left(R_T\right)\right] = \frac{\alpha}{\beta}\int TA\left(R_T\right)\pi\left(R_T; < R_T >\right) dR_T$. Because the transcriptional activity $TA\left(R_T\right)$was set to be identical across all indirect repression models, their total mean mRNA numbers—and thus their effective transcriptional activities under repressor fluctuation (i.e., the total mean multiplied by β/α)—are also identical across models: sole sequestration (red), combined sequestration and blocking (blue), and combined sequestration, blocking, and displacement (yellow). (c) Similarly, the total variance of the mRNA copy number can be calculated through the law of the total variance, $Var[M] = Var_\pi\left[E\left[M\middle|R_T\right]\right] + E_\pi\left[Var\left[M\middle|R_T\right]\right]$, where $Var\left[M|R_T\right]$ is the conditional variance of M for a given R_T. As $Var\left[M\middle|R_T\right]$ can be calculated as the product of the product of $E\left[M\middle|R_T\right]$ and the Fano factor $FF\left(R_T\right)$ in Table 2 (i.e., $\frac{\alpha}{\beta} TA\left(R_T\right) FF\left(R_T\right)$), the total variance of M becomes $Var[M] = \frac{\alpha}{\beta}\int\left(TA\left(R_T\right) - E[M]\right)^2\pi\left(R_T; < R_T >\right) dR_T + \frac{\alpha}{\beta}\int TA\left(R_T\right) FF\left(R_T\right)\pi\left(R_T; < R_T >\right) dR_T$. Because the transcriptional activity $TA\left(R_T\right)$ was set to be identical across all indirect repression models, the first term is also the same among models. In contrast, the second term differs due to variations in the Fano factor $FF\left(R_T\right)$. Consequently, consistent with its lowest Fano factor $FF\left(R_T\right)$, the model combining sequestration, blocking, and displacement exhibits the smallest overall mRNA variance, and thus the lowest overall mRNA Fano factor, demonstrating its robustness even under fluctuations in repressor copy number. (d) The number of activators can also fluctuate, when repressors bind to and promote the degradation of activators, as observed in systems such as the p53–MDM2 oscillator. To incorporate such fluctuations, we modeled the birth-death dynamics of the activator. Specifically, activators are produced at a rate α_A, degraded as free activators at a rate $\beta_A A/\Omega$, and further degraded in the form of repressor–activator complexes at a rate $\beta_{RA} R_A/\Omega$. Here, $A\left(A_T; R_T\right) = \frac{A_T - R_T - \Omega K_s + \sqrt{\left(A_T - R_T - \Omega K_s\right)^2 + 4\Omega K_s A_T}}{2} \approx \begin{cases} 0, & A_T \le R_T \\ A_T - R_T, & A_T > R_T \end{cases}$, and $R_A\left(A_T; R_T\right) = \frac{A_T + R_T + \Omega K_s - \sqrt{\left(A_T - R_T - \Omega K_s\right)^2 + 4\Omega K_s A_T}}{2} \approx \begin{cases} A_T, & A_T \le R_T \\ R_T, & A_T > R_T \end{cases}$ represent the number of free activators and repressor–activator complexes, respectively, as functions of the activator copy number (A_T) for a given R_T. Then, the probability distribution of A_T is governed by the following CME.
$\frac{dP\left(A_T\right)}{dt} = \alpha_A P\left(A_T - 1\right) + \left(\beta_A \frac{A\left(A_T + 1\right)}{\Omega} + \beta_{RA} \frac{R_A\left(A_T + 1\right)}{\Omega}\right) P\left(A_T + 1\right) - \left(\alpha_A + \beta_A \frac{A\left(A_T\right)}{\Omega} + \beta_{RA} \frac{R_A\left(A_T\right)}{\Omega}\right) P\left(A_T\right)$, where $P\left(A_T\right)$ denotes

the probability that the total number of activators is A_T, At stationary distribution (i.e., $\frac{dP(A_T)}{dt} = 0$), the CME satisfies $P(A_T+1) = \frac{\frac{\alpha_A\Omega}{\beta_{RA}}}{\frac{\beta_A}{\beta_{RA}}A(A_T;R_T)+R_A(A_T;R_T)}P(A_T) \approx \begin{cases} \frac{\frac{\alpha_A\Omega}{\beta_{RA}}}{A_T}P(A_T) \\ \frac{\frac{\alpha_A\Omega}{\beta_{RA}}}{\frac{\beta_A}{\beta_{RA}}A_T+\left(1-\frac{\beta_A}{\beta_{RA}}\right)R_T}P(A_T) \end{cases}$. Thus, the stationary distribution of A_T can be calculated recursively, and is determined by $\alpha_A\Omega/\beta_{RA}$ and β_{RA}/β_A, which represent the effective number of the activator and the relative degradation activator mediated by the repressor, respectively. Here, we simulated with $\alpha_A\Omega/\beta_{RA} = 1,000$ and $\beta_{RA}/\beta_A = 10$, while varying R_T to modulate the effective molar ratio $R_T^{eff} = R_T/\frac{\alpha_A\Omega}{\beta_{RA}}$. Notably, when the degradation rates of activators alone and in the complex are identical (i.e., $\beta_A = \beta_{RA}$), AT follows a simple Poisson distribution. In contrast, when the repressor promotes activator degradation by binding (i.e., $\beta_A < \beta_{RA}$), the stationary distribution of A_T deviates from Poisson. (e) With the calculated non-Poisson distribution of A_T ($\pi(A_T; R_T, \frac{\alpha_A\Omega}{\beta_{RA}}, \frac{\beta_{RA}}{\beta_A})$), the total mean of M is given by $E[M] = E_\pi\left[\frac{\alpha}{\beta}TA(A_T)\right] = \frac{\alpha}{\beta}\int TA(A_T)\,\pi\left(A_T; R_T, \frac{\alpha_A\Omega}{\beta_{RA}}, \frac{\beta_{RA}}{\beta_A}\right)dA_T$. Because the transcriptional activity $TA(A_T)$ was set to be identical across all indirect repression models, their total mean mRNA numbers—and thus their effective transcriptional activities under activator fluctuation (i.e., the total mean multiplied by β/α)—are also identical across models: sole sequestration (red), combined sequestration and blocking (blue), and combined sequestration, blocking, and displacement (yellow). (f) Similarly, the total variance of the mRNA copy number can be calculated through the law of the total variance, $Var[M] = \frac{\alpha}{\beta}\int(TA(A_T)-E[M])^2\,\pi\left(A_T; R_T, \frac{\alpha_A\Omega}{\beta_{RA}}, \frac{\beta_{RA}}{\beta_A}\right)dR_T + \frac{\alpha}{\beta}\int TA(A_T)\,FF(A_T)\,\pi\left(A_T; R_T, \frac{\alpha_A\Omega}{\beta_{RA}}, \frac{\beta_{RA}}{\beta_A}\right)dA_T$. Because the transcriptional activity $TA(A_T)$ was set to be identical across all indirect repression models, the first term is also the same among models. In contrast, the second term differs due to variations in the Fano factor $FF(A_T)$. Consequently, consistent with its lowest Fano factor $FF(A_T)$, the model combining sequestration, blocking, and displacement exhibits the smallest overall mRNA variance, and thus the lowest overall mRNA Fano factor, demonstrating its robustness even under fluctuations in activator copy number.
(TIF)

S5 Fig. Systematic evaluation of the effects of indirect repression mechanisms on ultrasensitivity of transcriptional activity and overall noise level. (a - b) Heatmaps showing the ultrasensitivity of transcriptional activity and the overall noise level, quantified by the Hill coefficient (a) and the area under the Fano factor curve (AUC) over a range of $\widetilde{R_T}$ from 10^{-1} to 10^{1} (b), respectively, by varying the dissociation constants K_a and K_s in the three indirect repression models. In the sole sequestration model, strong sequestration (i.e., $K_s \ll K_a$) promoted high ultrasensitivity (a(i)) but was accompanied by elevated noise levels (b(i)). Incorporating blocking, with $K_b = 10^{-3}$, maintained a similar level of ultrasensitivity as in the sole sequestration case (a(ii)), while reducing the overall noise (b(ii)), indicating that the addition of blocking dampens fluctuations without compromising sensitivity. Further strengthening the blocking ($K_b = 10^{-4}$) lowered the noise even more (b(iii)) without loss of ultrasensitivity (a(iii)). Regardless of blocking strength, adding displacement, with its rate set to $K_d = K_aK_b/K_s$ to maintain comparable ultrasensitivity (a(iv-v)), led to additional noise reduction (b(iv-v)), demonstrating cumulative noise suppression through cooperative multiple repressions. Moreover, stronger displacement ($K_d = 10K_aK_b/K_s$) produced higher ultrasensitivity (a(vi-vii)) with sustained low noise (b(vi-vii)) compared to the weaker displacement ($K_d = K_aK_b/K_s$; a(iv-v) and b(iv-v)). Taken together, the sequential addition and strengthening of repression mechanisms progressively reduced noise while retaining or amplifying ultrasensitivity.
(TIF)

Author contributions

Conceptualization: Eui Min Jeong, Chang Yoon Chung, Jae Kyoung Kim.

Data curation: Eui Min Jeong, Chang Yoon Chung.

Formal analysis: Eui Min Jeong, Chang Yoon Chung, Jae Kyoung Kim.

Funding acquisition: Eui Min Jeong, Jae Kyoung Kim.

Investigation: Eui Min Jeong, Chang Yoon Chung, Jae Kyoung Kim.

Methodology: Eui Min Jeong, Chang Yoon Chung, Jae Kyoung Kim.

Project administration: Jae Kyoung Kim.

Resources: Eui Min Jeong, Jae Kyoung Kim.

Software: Eui Min Jeong, Chang Yoon Chung.

Supervision: Jae Kyoung Kim.

Validation: Eui Min Jeong, Jae Kyoung Kim.

Visualization: Eui Min Jeong, Chang Yoon Chung.

Writing – original draft: Eui Min Jeong, Chang Yoon Chung, Jae Kyoung Kim.

Writing – review & editing: Eui Min Jeong, Chang Yoon Chung, Jae Kyoung Kim.

References

1. Ferrell JE Jr, Ha SH. Ultrasensitivity part III: cascades, bistable switches, and oscillators. Trends Biochem Sci. 2014;39(12):612–8. https://doi.org/10.1016/j.tibs.2014.10.002 PMID: 25456048
2. Ferrell JE Jr, Ha SH. Ultrasensitivity part I: Michaelian responses and zero-order ultrasensitivity. Trends Biochem Sci. 2014;39(10):496–503. https://doi.org/10.1016/j.tibs.2014.08.003 PMID: 25240485
3. Novák B, Tyson JJ. Design principles of biochemical oscillators. Nat Rev Mol Cell Biol. 2008;9(12):981–91. https://doi.org/10.1038/nrm2530 PMID: 18971947
4. Ferrell JE Jr, Tsai TY-C, Yang Q. Modeling the cell cycle: why do certain circuits oscillate? Cell. 2011;144(6):874–85. https://doi.org/10.1016/j.cell.2011.03.006 PMID: 21414480
5. Ha SH, Ferrell JE Jr. Thresholds and ultrasensitivity from negative cooperativity. Science. 2016;352(6288):990–3. https://doi.org/10.1126/science.aad5937 PMID: 27174675
6. Stefan MI, Le Novère N. Cooperative binding. PLoS Comput Biol. 2013;9(6):e1003106. https://doi.org/10.1371/journal.pcbi.1003106 PMID: 23843752
7. Achsel T, Bagni C. Cooperativity in RNA-protein interactions: the complex is more than the sum of its partners. Curr Opin Neurobiol. 2016;39:146–51. https://doi.org/10.1016/j.conb.2016.06.007 PMID: 27352301
8. de Vink PJ, Andrei SA, Higuchi Y, Ottmann C, Milroy L-G, Brunsveld L. Cooperativity basis for small-molecule stabilization of protein-protein interactions. Chem Sci. 2019;10(10):2869–74. https://doi.org/10.1039/c8sc05242e PMID: 30996864
9. Zhang Q, Bhattacharya S, Andersen ME. Ultrasensitive response motifs: basic amplifiers in molecular signalling networks. Open Biol. 2013;3(4):130031. https://doi.org/10.1098/rsob.130031 PMID: 23615029
10. Bintu L, Buchler NE, Garcia HG, Gerland U, Hwa T, Kondev J, et al. Transcriptional regulation by the numbers: applications. Curr Opin Genet Dev. 2005;15(2):125–35. https://doi.org/10.1016/j.gde.2005.02.006 PMID: 15797195
11. Ferrell JE Jr, Ha SH. Ultrasensitivity part II: multisite phosphorylation, stoichiometric inhibitors, and positive feedback. Trends Biochem Sci. 2014;39(11):556–69. https://doi.org/10.1016/j.tibs.2014.09.003 PMID: 25440716
12. Buchler NE, Cross FR. Protein sequestration generates a flexible ultrasensitive response in a genetic network. Mol Syst Biol. 2009;5:272. https://doi.org/10.1038/msb.2009.30 PMID: 19455136
13. Buchler NE, Louis M. Molecular titration and ultrasensitivity in regulatory networks. J Mol Biol. 2008;384(5):1106–19. https://doi.org/10.1016/j.jmb.2008.09.079 PMID: 18938177
14. Kim JK. Protein sequestration versus Hill-type repression in circadian clock models. IET Syst Biol. 2016;10(4):125–35. https://doi.org/10.1049/iet-syb.2015.0090 PMID: 27444022
15. Beesley S, Kim DW, D'Alessandro M, Jin Y, Lee K, Joo H, et al. Wake-sleep cycles are severely disrupted by diseases affecting cytoplasmic homeostasis. Proc Natl Acad Sci U S A. 2020;117(45):28402–11. https://doi.org/10.1073/pnas.2003524117 PMID: 33106420
16. Chae SJ, Kim DW, Lee S, Kim JK. Spatially coordinated collective phosphorylation filters spatiotemporal noises for precise circadian timekeeping. iScience. 2023;26(4):106554. https://doi.org/10.1016/j.isci.2023.106554 PMID: 37123226
17. Gotoh T, Kim JK, Liu J, Vila-Caballer M, Stauffer PE, Tyson JJ, et al. Model-driven experimental approach reveals the complex regulatory distribution of p53 by the circadian factor Period 2. Proc Natl Acad Sci U S A. 2016;113(47):13516–21. https://doi.org/10.1073/pnas.1607984113 PMID: 27834218

18. Jeong EM, Kwon M, Cho E, Lee SH, Kim H, Kim EY, et al. Systematic modeling-driven experiments identify distinct molecular clockworks underlying hierarchically organized pacemaker neurons. Proc Natl Acad Sci U S A. 2022;119(8):e2113403119. https://doi.org/10.1073/pnas.2113403119 PMID: 35193959
19. D'Alessandro M, Beesley S, Kim JK, Jones Z, Chen R, Wi J, et al. Stability of Wake-Sleep Cycles Requires Robust Degradation of the PERIOD Protein. Curr Biol. 2017;27(22):3454–3467.e8. https://doi.org/10.1016/j.cub.2017.10.014 PMID: 29103939
20. Kim SY, Ferrell JE Jr. Substrate competition as a source of ultrasensitivity in the inactivation of Wee1. Cell. 2007;128(6):1133–45. https://doi.org/10.1016/j.cell.2007.01.039 PMID: 17382882
21. Jeong EM, Song YM, Kim JK. Combined multiple transcriptional repression mechanisms generate ultrasensitivity and oscillations. Interface Focus. 2022;12(3):20210084. https://doi.org/10.1098/rsfs.2021.0084 PMID: 35450279
22. Jeong EM, Kim JK. A robust ultrasensitive transcriptional switch in noisy cellular environments. NPJ Syst Biol Appl. 2024;10(1):30. https://doi.org/10.1038/s41540-024-00356-2 PMID: 38493227
23. Milo R, Phillips R. Cell biology by the numbers. 2015.
24. Williamson MP. Protein Binding: A Fuzzy Concept. Life (Basel). 2023;13(4):855. https://doi.org/10.3390/life13040855 PMID: 37109384
25. Yao X, Heidebrecht BL, Chen J, Tyson JJ. Mathematical analysis of robustness of oscillations in models of the mammalian circadian clock. PLoS Comput Biol. 2022;18(3):e1008340. https://doi.org/10.1371/journal.pcbi.1008340 PMID: 35302984
26. Bintu L, Buchler NE, Garcia HG, Gerland U, Hwa T, Kondev J, et al. Transcriptional regulation by the numbers: models. Curr Opin Genet Dev. 2005;15(2):116–24. https://doi.org/10.1016/j.gde.2005.02.007 PMID: 15797194
27. Gillespie DT. Exact stochastic simulation of coupled chemical reactions. J Phys Chem. 1977;81(25):2340–61. https://doi.org/10.1021/j100540a008
28. Sanchez A, Garcia HG, Jones D, Phillips R, Kondev J. Effect of promoter architecture on the cell-to-cell variability in gene expression. PLoS Comput Biol. 2011;7(3):e1001100. https://doi.org/10.1371/journal.pcbi.1001100 PMID: 21390269
29. Bergqvist S, Alverdi V, Mengel B, Hoffmann A, Ghosh G, Komives EA. Kinetic enhancement of NF-kappaBxDNA dissociation by IkappaBalpha. Proc Natl Acad Sci U S A. 2009;106(46):19328–33. https://doi.org/10.1073/pnas.0908797106 PMID: 19887633
30. Zou R, Zhou Y, Wang Y, Kuang G, Ågren H, Wu J, et al. Free Energy Profile and Kinetics of Coupled Folding and Binding of the Intrinsically Disordered Protein p53 with MDM2. J Chem Inf Model. 2020;60(3):1551–8. https://doi.org/10.1021/acs.jcim.9b00920 PMID: 32053358
31. Sharova LV, Sharov AA, Nedorezov T, Piao Y, Shaik N, Ko MSH. Database for mRNA half-life of 19 977 genes obtained by DNA microarray analysis of pluripotent and differentiating mouse embryonic stem cells. DNA Res. 2009;16(1):45–58. https://doi.org/10.1093/dnares/dsn030 PMID: 19001483
32. Wang C, Liu H. Factors influencing degradation kinetics of mRNAs and half-lives of microRNAs, circRNAs, lncRNAs in blood in vitro using quantitative PCR. Sci Rep. 2022;12(1):7259. https://doi.org/10.1038/s41598-022-11339-w PMID: 35508612
33. Gaston K, Jayaraman PS. Transcriptional repression in eukaryotes: repressors and repression mechanisms. Cell Mol Life Sci. 2003;60(4):721–41. https://doi.org/10.1007/s00018-003-2260-3 PMID: 12785719
34. Renkawitz R. Transcriptional repression in eukaryotes. Trends Genet. 1990;6(6):192–7. https://doi.org/10.1016/0168-9525(90)90176-7 PMID: 2196723
35. Kim JK, Forger DB. A mechanism for robust circadian timekeeping via stoichiometric balance. Mol Syst Biol. 2012;8:630. https://doi.org/10.1038/msb.2012.62 PMID: 23212247
36. Engelmann N, Molderings M, Koeppl H. Tuning Ultrasensitivity in Genetic Logic Gates Using Antisense RNA Feedback. ACS Synth Biol. 2025;14(5):1425–36. https://doi.org/10.1021/acssynbio.4c00438 PMID: 40335038
37. Khetan N, Zuckerman B, Calia GP, Chen X, Garcia Arceo X, Weinberger LS. Single-cell RNA sequencing algorithms underestimate changes in transcriptional noise compared to single-molecule RNA imaging. Cell Rep Methods. 2024;4(12):100933. https://doi.org/10.1016/j.crmeth.2024.100933 PMID: 39662473
38. Menet JS, Abruzzi KC, Desrochers J, Rodriguez J, Rosbash M. Dynamic PER repression mechanisms in the Drosophila circadian clock: from on-DNA to off-DNA. Genes Dev. 2010;24(4):358–67. https://doi.org/10.1101/gad.1883910 PMID: 20159956
39. Ye R, Selby CP, Chiou Y-Y, Ozkan-Dagliyan I, Gaddameedhi S, Sancar A. Dual modes of CLOCK:BMAL1 inhibition mediated by Cryptochrome and Period proteins in the mammalian circadian clock. Genes Dev. 2014;28(18):1989–98. https://doi.org/10.1101/gad.249417.114 PMID: 25228643
40. Chiou Y-Y, Yang Y, Rashid N, Ye R, Selby CP, Sancar A. Mammalian Period represses and de-represses transcription by displacing CLOCK-BMAL1 from promoters in a Cryptochrome-dependent manner. Proc Natl Acad Sci U S A. 2016;113(41):E6072–9. https://doi.org/10.1073/pnas.1612917113 PMID: 27688755
41. Cao X, Yang Y, Selby CP, Liu Z, Sancar A. Molecular mechanism of the repressive phase of the mammalian circadian clock. Proc Natl Acad Sci U S A. 2021;118(2):e2021174118. https://doi.org/10.1073/pnas.2021174118 PMID: 33443219
42. Takahashi JS. Transcriptional architecture of the mammalian circadian clock. Nat Rev Genet. 2017;18(3):164–79. https://doi.org/10.1038/nrg.2016.150 PMID: 27990019
43. Partch CL. Orchestration of Circadian Timing by Macromolecular Protein Assemblies. J Mol Biol. 2020;432(12):3426–48. https://doi.org/10.1016/j.jmb.2019.12.046 PMID: 31945377

44. Otobe Y, Jeong EM, Ito S, Shinohara Y, Kurabayashi N, Aiba A, et al. Phosphorylation of DNA-binding domains of CLOCK-BMAL1 complex for PER-dependent inhibition in circadian clock of mammalian cells. Proc Natl Acad Sci U S A. 2024;121(23):e2316858121. https://doi.org/10.1073/pnas.2316858121 PMID: 38805270
45. Potoyan DA, Zheng W, Komives EA, Wolynes PG. Molecular stripping in the NF-κB/IκB/DNA genetic regulatory network. Proc Natl Acad Sci U S A. 2016;113(1):110–5. https://doi.org/10.1073/pnas.1520483112 PMID: 26699500
46. Cross B, Chen L, Cheng Q, Li B, Yuan Z-M, Chen J. Inhibition of p53 DNA binding function by the MDM2 protein acidic domain. J Biol Chem. 2011;286(18):16018–29. https://doi.org/10.1074/jbc.M111.228981 PMID: 21454483
47. Chen J. The Cell-Cycle Arrest and Apoptotic Functions of p53 in Tumor Initiation and Progression. Cold Spring Harb Perspect Med. 2016;6(3):a026104. https://doi.org/10.1101/cshperspect.a026104 PMID: 26931810
48. Song YM, Campbell S, Shiau L, Kim JK, Ott W. Noisy Delay Denoises Biochemical Oscillators. Phys Rev Lett. 2024;132(7):078402. https://doi.org/10.1103/PhysRevLett.132.078402 PMID: 38427894
49. Cao Y, Wang H, Ouyang Q, Tu Y. The free energy cost of accurate biochemical oscillations. Nat Phys. 2015;11(9):772–8. https://doi.org/10.1038/nphys3412 PMID: 26566392
50. Koch AA, Bagnall JS, Smyllie NJ, Begley N, Adamson AD, Fribourgh JL, et al. Quantification of protein abundance and interaction defines a mechanism for operation of the circadian clock. Elife. 2022;11:e73976. https://doi.org/10.7554/eLife.73976 PMID: 35285799
51. Fischer M. Census and evaluation of p53 target genes. Oncogene. 2017;36(28):3943–56. https://doi.org/10.1038/onc.2016.502 PMID: 28288132
52. Zhao M, Joy J, Zhou W, De S, Wood WH 3rd, Becker KG, et al. Transcriptional outcomes and kinetic patterning of gene expression in response to NF-κB activation. PLoS Biol. 2018;16(9):e2006347. https://doi.org/10.1371/journal.pbio.2006347 PMID: 30199532
53. Lee T-H, Maheshri N. A regulatory role for repeated decoy transcription factor binding sites in target gene expression. Mol Syst Biol. 2012;8:576. https://doi.org/10.1038/msb.2012.7 PMID: 22453733
54. Dey S, Soltani M, Singh A. Enhancement of gene expression noise from transcription factor binding to genomic decoy sites. Sci Rep. 2020;10(1):9126. https://doi.org/10.1038/s41598-020-65750-2 PMID: 32499583
55. Guo X, Adelaja A, Singh A, Wollman R, Hoffmann A. Modeling heterogeneous signaling dynamics of macrophages reveals principles of information transmission in stimulus responses. Nat Commun. 2025;16(1):5986. https://doi.org/10.1038/s41467-025-60901-3 PMID: 40593748
56. Zambrano S, De Toma I, Piffer A, Bianchi ME, Agresti A. NF-κB oscillations translate into functionally related patterns of gene expression. Elife. 2016;5:e09100. https://doi.org/10.7554/eLife.09100 PMID: 26765569
57. Geva-Zatorsky N, Rosenfeld N, Itzkovitz S, Milo R, Sigal A, Dekel E, et al. Oscillations and variability in the p53 system. Mol Syst Biol. 2006;2. https://doi.org/10.1038/msb4100068 PMID: 16773083
58. Xie J, Zhang L, Liu B, Liang X, Shi J. Single-cell analysis of p53 transitional dynamics unravels stimulus- and cell type-dependent signaling output motifs. BMC Biol. 2022;20(1):85. https://doi.org/10.1186/s12915-022-01290-7 PMID: 35410287
59. Kellogg RA, Tian C, Lipniacki T, Quake SR, Tay S. Digital signaling decouples activation probability and population heterogeneity. Elife. 2015;4:e08931. https://doi.org/10.7554/eLife.08931 PMID: 26488364
60. Bolognesi B, Lehner B. Reaching the limit. Elife. 2018;7:e39804. https://doi.org/10.7554/eLife.39804 PMID: 30095407
61. Dekel E, Alon U. Optimality and evolutionary tuning of the expression level of a protein. Nature. 2005;436(7050):588–92. https://doi.org/10.1038/nature03842 PMID: 16049495
62. Frei T, Cella F, Tedeschi F, Gutiérrez J, Stan G-B, Khammash M, et al. Characterization and mitigation of gene expression burden in mammalian cells. Nat Commun. 2020;11(1):4641. https://doi.org/10.1038/s41467-020-18392-x PMID: 32934213
63. Todeschini A-L, Georges A, Veitia RA. Transcription factors: specific DNA binding and specific gene regulation. Trends Genet. 2014;30(6):211–9. https://doi.org/10.1016/j.tig.2014.04.002 PMID: 24774859
64. Estrada J, Wong F, DePace A, Gunawardena J. Information Integration and Energy Expenditure in Gene Regulation. Cell. 2016;166(1):234–44. https://doi.org/10.1016/j.cell.2016.06.012 PMID: 27368104
65. Fei C, Cao Y, Ouyang Q, Tu Y. Design principles for enhancing phase sensitivity and suppressing phase fluctuations simultaneously in biochemical oscillatory systems. Nat Commun. 2018;9(1):1434. https://doi.org/10.1038/s41467-018-03826-4 PMID: 29651016
66. Markevich NI, Hoek JB, Kholodenko BN. Signaling switches and bistability arising from multisite phosphorylation in protein kinase cascades. J Cell Biol. 2004;164(3):353–9. https://doi.org/10.1083/jcb.200308060 PMID: 14744999
67. Li C-J, Liau ES, Lee Y-H, Huang Y-Z, Liu Z, Willems A, et al. MicroRNA governs bistable cell differentiation and lineage segregation via a noncanonical feedback. Mol Syst Biol. 2021;17(4):e9945. https://doi.org/10.15252/msb.20209945 PMID: 33890404
68. Quattrone A, Dassi E. The Architecture of the Human RNA-Binding Protein Regulatory Network. iScience. 2019;21:706–19. https://doi.org/10.1016/j.isci.2019.10.058 PMID: 31733516
69. Mukherji S, Ebert MS, Zheng GXY, Tsang JS, Sharp PA, van Oudenaarden A. MicroRNAs can generate thresholds in target gene expression. Nat Genet. 2011;43(9):854–9. https://doi.org/10.1038/ng.905 PMID: 21857679
70. Goldbeter A, Koshland DE Jr. An amplified sensitivity arising from covalent modification in biological systems. Proc Natl Acad Sci U S A. 1981;78(11):6840–4. https://doi.org/10.1073/pnas.78.11.6840 PMID: 6947258

71. Jia C, Li Y. Analytical Time-Dependent Distributions for Gene Expression Models With Complex Promoter Switching Mechanisms. SIAM J Appl Math. 2023;83(4):1572–602. https://doi.org/10.1137/22m147219x
72. Jia C, Qian H, Zhang MQ. Exact Power Spectrum in a Minimal Hybrid Model of Stochastic Gene Expression Oscillations. SIAM J Appl Math. 2024;84(3):1204–26. https://doi.org/10.1137/23m1560914
73. Kim JK, Josić K, Bennett MR. The validity of quasi-steady-state approximations in discrete stochastic simulations. Biophys J. 2014;107(3):783–93. https://doi.org/10.1016/j.bpj.2014.06.012 PMID: 25099817
74. Song YM, Hong H, Kim JK. Universally valid reduction of multiscale stochastic biochemical systems using simple non-elementary propensities. PLoS Comput Biol. 2021;17(10):e1008952. https://doi.org/10.1371/journal.pcbi.1008952 PMID: 34662330
75. Kim JK. Tick, Tock, Circadian Clocks. In: Kraikivski P, editor. Case Studies in Systems Biology. Cham: Springer International Publishing; 2021:79–94.
76. Song YM, Lee K, Kim JK. Validity of the total quasi-steady-state approximation in stochastic biochemical reaction networks. Journal of the Korean Society for Industrial and Applied Mathematics. 2025;1–15.